© 2019. Published by The Company of Biologists Ltd | Journal of Cell Science (2019) 132, jcs227447. doi:10.1242/jcs.227447

RESEARCH ARTICLE

Increasing ergosterol levels delays formin-dependent assembly of F-actin cables and disrupts division plane positioning in fission yeast

Federica Arbizzani[1], Sergio A. Rincon[1,2,*,‡] and Anne Paoletti[1,*,‡]

ABSTRACT

In most eukaryotes, cytokinesis is mediated by the constriction of a contractile acto-myosin ring (CR), which promotes the ingression of the cleavage furrow. Many components of the CR interact with plasma membrane lipids suggesting that lipids may regulate CR assembly and function. Although there is clear evidence that phosphoinositides play an important role in cytokinesis, much less is known about the role of sterols in this process. Here, we studied how sterols influence division plane positioning and CR assembly in fission yeast. We show that increasing ergosterol levels in the plasma membrane blocks the assembly of F-actin cables from cytokinetic precursor nodes, preventing their compaction into a ring. Abnormal F-actin cables form after a delay, leading to randomly placed septa. Since the formin Cdc12 was detected on cytokinetic precursors and the phenotype can be partially rescued by inhibiting the Arp2/3 complex, which competes with formins for F-actin nucleation, we propose that ergosterol may inhibit formin dependent assembly of F-actin cables from cytokinetic precursors.

KEY WORDS: Actin, Contractile ring, Cytokinesis, Fission yeast, Formin, Sterol-rich domain

INTRODUCTION

Cell division is an essential process required for the proliferation of unicellular organisms as well as for the development of multicellular organisms and cell renewal within tissues. Its final step, cytokinesis, ensures the physical separation of the two daughter cells. Defective control of this step can either lead to cell death or to aneuploidy, and can contribute to cancer progression (Fujiwara et al., 2005; Lacroix and Maddox, 2012; Storchova and Pellman, 2004). Cytokinesis is therefore under the control of very tight spatial and temporal regulatory mechanisms.

In most eukaryotes, cytokinesis relies on an acto-myosin based contractile ring (CR), which assembles at the division site and constricts to cause the invagination of the plasma membrane and promote the ingression of the cleavage furrow between the two sets of segregating chromosomes. Fission yeast (*Schizosaccharomyces pombe*) has provided crucial insights into the molecular mechanisms of CR assembly. In this model organism, CR assembly is initiated by cytokinetic precursors organized since interphase on the medial cortex of the cell by the SAD kinase Cdr2 (Akamatsu et al., 2017; Moseley et al., 2009; Pollard and Wu, 2010; Rincon and Paoletti, 2016; Willet et al., 2015b; Wu et al., 2006). Medial positioning of these nodes contributes to division plane positioning and is ensured by negative signalling by the gradient of the DYRK kinase Pom1 emanating from the cell tips (Celton-Morizur et al., 2006; Martin and Berthelot-Grosjean, 2009; Moseley et al., 2009; Padte et al., 2006; Rincon et al., 2014). These cytokinetic precursors contain several non-essential cytokinetic ring components, such as the anillin-like protein Mid1, Blt1, Gef2, Klp8 and Nod1 (Goss et al., 2014; Guzman-Vendrell et al., 2013; Jourdain et al., 2013; Martin and Berthelot-Grosjean, 2009; Moseley et al., 2009; Ye et al., 2012; Zhu et al., 2013). Upon mitotic entry, positive signalling from the medially placed nucleus, mediated by the polo-like kinase Plo1-induced export from the nucleus of the anillin-like protein Mid1, reinforces division plane positioning in the cell middle (Almonacid et al., 2009), while Cdr2 dissociates from the cytokinetic precursors in a septation initiation network (SIN)-dependent manner (Akamatsu et al., 2014; Rincon et al., 2017). Plo1 also activates Mid1, which becomes competent for the sequential recruitment of essential ring components (Almonacid et al., 2011): Mid1 first engages the IQGAP protein Rng2 and myosin II light chain Cdc4, heavy chain Myo2 and regulatory light chain Rlc1. Mid1 also contributes directly to the recruitment of the F-BAR protein Cdc15 (Laporte et al., 2011). Rng2 and myosin II, together with Cdc15 collaborate in the recruitment of the formin Cdc12, which nucleates F-actin cables required for CR assembly (Coffman et al., 2009, 2013; Laporte et al., 2011; Padmanabhan et al., 2011; Willet et al., 2015a; Wu et al., 2003, 2006). This step is necessary for myosin II-dependent node compaction into a tight acto-myosin ring in a mechanism modeled under the name of search-capture-pull-release (Ojkic et al., 2011; Vavylonis et al., 2008).

In parallel to CR assembly, modifications in the lipid composition of the plasma membrane take place at the division site with a functional impact on cytokinesis (Atilla-Gokcumen et al., 2014; Echard and Burgess, 2014). So far, major studies have focused on phosphoinositides, which play key roles in membrane trafficking and cytoskeleton rearrangements. In particular, in human cells, phosphatidylinositol 4,5-bisphosphate [PI(4,5)P_2] enrichment at the cytokinesis furrow and early intercellular bridges is crucial for F-actin remodeling by RhoA, anillin and septins, whereas its hydrolysis by the PIP_2 phosphatase OCRL is necessary for abscission, avoiding abnormal F-actin accumulation at cytokinesis bridges (Cauvin and Echard, 2015; Dambournet et al., 2011; Echard, 2012).

In fission yeast, only sparse data are available on the role of membrane lipids in cytokinesis. First, the correct localization of the PI4 kinase Stt4 by its scaffolding subunit Efr3 (Baird et al., 2008) was recently shown to play a role in the spatial regulation of

[1]Institut Curie, PSL University, CNRS UMR 144, 75005 Paris, France. [2]Instituto de Biología Funcional y Genómica and Departamento de Microbiología y Genética, Consejo Superior de Investigaciones Científicas (CSIC)/Universidad de Salamanca, Salamanca 37007, Spain.
*These authors contributed equally to this work

‡Authors for correspondence (anne.paoletti@curie.fr; sarpadilla@usal.es)

S.A.R., 0000-0002-7169-2097; A.P., 0000-0002-9004-559X

Received 2 November 2018; Accepted 31 May 2019

Journal of Cell Science (2019) 132, jcs227447. doi:10.1242/jcs.227447

cytokinesis by preventing the CR sliding toward one cell tip during anaphase (Snider et al., 2017). Similarly, defects in the spatial regulation of cytokinesis at the beginning of mitosis have been reported in the PI-5 kinase *its3-1* mutant, characterized by reduced levels of phosphatidylinositol 3,5-bisphosphate [$PI(3,5)P_2$] (Snider et al., 2018). Second, defects in cytokinesis as well as cell morphology and cell wall organization were observed in a mutant of Pps1, involved in phosphatidylserine (PS) synthesis (Matsuo et al., 2007). Third, defects in sphingolipid hydrolysis into ceramide in *css1* mutant were shown to induce defects in cell wall and septum formation, due to the accumulation of α- and β-glucans in the periplasmic space, with cell division arrest and a lethal outcome (Feoktistova et al., 2001).

Some data also point out a role for sterols in the regulation of cytokinesis (Wachtler et al., 2003). Sterols are synthesized and mature in the ER by a cascade of coupled enzymatic reactions. The final metabolic product, cholesterol in the case of animal cells and ergosterol in fungi, is then transported to the plasma membrane where it forms liquid-ordered domains by interacting preferentially with sphingolipids, which have recognized roles in signal transduction, vesicular sorting and polarity (Rajendran and Simons, 2005). Key factors for the formation of sterol-rich domains (SRDs) are the F-BAR protein Cdc15 and the type I myosin Myo1, which interact with one another, binding preferentially to acidic phospholipids (Alvarez et al., 2007; Carnahan and Gould, 2003; Takeda and Chang, 2005; Takeda et al., 2004). Besides, SRDs redistribute from growing cell tips in interphase, where they act as scaffolds for polarity factors and the growth machinery (Makushok et al., 2016), to the division site in mitosis (Wachtler et al., 2003).

Interestingly, Wachtler et al. (2003) found that the overexpression of Erg25, a C-4 sterol-methyl-oxidase of the ergosterol synthesis pathway, could alter ergosterol distribution within the cell and disrupt CR positioning, leading to the formation of random positioned and misshapen septa (Wachtler et al., 2003). This phenotype is strikingly similar to the phenotype produced by the deletion of the main division plane position factor Mid1, which is associated with the cytokinetic precursors described above.

Here, by combining fission yeast genetics with live-cell imaging of CR assembly from cytokinetic precursors, we show that increasing ergosterol levels does not affect the assembly or distribution of cytokinetic precursors, nor the recruitment of the IQGAP protein Rng2, myosin II or the F-BAR protein Cdc15, at mitotic entry. Instead, it inhibits the assembly of medial F-actin cables from cytokinetic precursors preventing node compaction into a tight ring. Randomly positioned F-actin cables finally emerge, with a long delay compared to the wild-type situation, leading to abnormally placed septa. Analysis of the formin Cdc12 that nucleates F-actin cables from cytokinetic precursors revealed that its recruitment to the medial cortex is not abolished in these circumstances, although we cannot exclude the possibility that its amount is reduced. Since the stability of F-actin cables was not altered altogether and the phenotype could be partially rescued by inhibition of Arp2/3, which competes with formins, we propose that increasing ergosterol levels in the plasma membrane may inhibit the activity of the formin Cdc12.

RESULTS

To understand how ergosterol homeostasis may influence division plane positioning, we decided to reproduce Erg25 overexpression (denoted Erg25 OE) from a multicopy plasmid under the control of the thiamine-repressible *nmt1* promoter (Maundrell, 1993). Septum organization was analysed by staining cells with the cell wall dye Calcofluor after thiamine removal to induce Erg25 OE (Fig. 1A). We found that 85.6±4.3% (mean±s.d.) of cells overexpressing Erg25 had abnormal septa compared to 1.9±0.2% of control cells (Fig. 1B).

To determine the ergosterol distribution pattern in this context, cells were stained with the ergosterol-specific dye filipin. As expected, an altered pattern of distribution of ergosterol was observed upon Erg25 OE, with increased levels of ergosterol not only at the cell tips where it normally accumulates (Takeda et al., 2004; Wachtler et al., 2003), but also around the whole-cell periphery, including at the medial cell cortex (Fig. 1C). Accordingly, the intensity of filipin staining in late G2 cells, ranging from 11.5 to 13.5 µm, in length showed a 1.7-fold increase of sterols at the cell tips, and a 1.5-fold increase of sterols in the cell middle, compared to the wild-type situation (n=15 for both control and Erg25 OE cells; Fig. 1D). Finally, in dividing cells, filipin was concentrated at the division site, which was abnormally shaped upon Erg25 OE. These data confirms that ergosterol levels are increased in the plasma membrane upon Erg25 OE, including in the medial region of the cell where CR assembly takes place at mitotic entry.

Next, in order to verify whether the defects in division plane position were due to ergosterol enrichment, we treated control and Erg25 overexpressing cells with miconazole. This drug inhibits Erg11, a lanosterol 14-α demethylase that functions immediately upstream of Erg25 in the ergosterol synthesis pathway (Fig. S1A) (Löffler et al., 1997; Marichal et al., 1999; Rippon and Fromtling, 1993; Sanglard et al., 1998; Sheehan et al., 1999). Miconazole induced a reduction of ∼80% in the number of abnormally shaped septa upon Erg25 OE (Fig. 1E; Fig. S1B). In parallel, we also overexpressed Erg25 in cells lacking *erg6* (*erg6*Δ), which encodes a protein acting immediately downstream of Erg25 in the ergosterol synthesis pathway (Fig. S1A) (Bard et al., 1996; Iwaki et al., 2008). The number of abnormally shaped septa was reduced from ∼85% in Erg25 OE cells to less than 40% in the *erg6*Δ mutant (Fig. S1C), consistent with the suppression of the phenotype induced by miconazole. The partial suppression seen in the *erg6*Δ mutant might be due to alternative biosynthetic pathway allowing ergosterol production from zymosterol independently of *erg6*. From these experiments, we conclude that ring positioning defects produced by Erg25 OE require an active sterol synthesis pathway and are effectively related to sterol overproduction, excluding other unrelated functional defects that Erg25 OE might have caused.

We next determined the localization of Erg25 by fusing it to the green fluorescent tag ENVY (Slubowski et al., 2015) at its C-terminus. Fluorescence microscopy revealed that Erg25 has both a perinuclear and a peripheral distribution around the cell (Fig. S1D), reminiscent of the endoplasmic reticulum (ER) distribution. Accordingly, when Erg25–ENVY was expressed together with the ER marker Elo2, a fatty acid elongase (labelled as ER-mCherry in Fig. S1D), we found that the two proteins perfectly colocalized. This result is in agreement with the fact that sterol metabolism takes place in this organelle (Jacquier and Schneiter, 2012).

We next wanted to determine whether the distribution of Erg25 was altered upon its overexpression. To do so, we ectopically overexpressed Erg25 in the endogenously producing Erg25–ENVY strain. In interphase cells, the protein lost its strong enrichment around the nucleus and the cell surface, and formed irregular patterns in a medial cytoplasmic zone (Fig. S1E). Quantification of this phenotype showed that 82.6±3.3% of interphase cells overexpressing Erg25 displayed an abnormal distribution of Erg25 in comparison to none in the control (Fig. S1F). This result indicates that Erg25 OE alters the organization of the ER.

Journal of Cell Science (2019) 132, jcs227447. doi:10.1242/jcs.227447

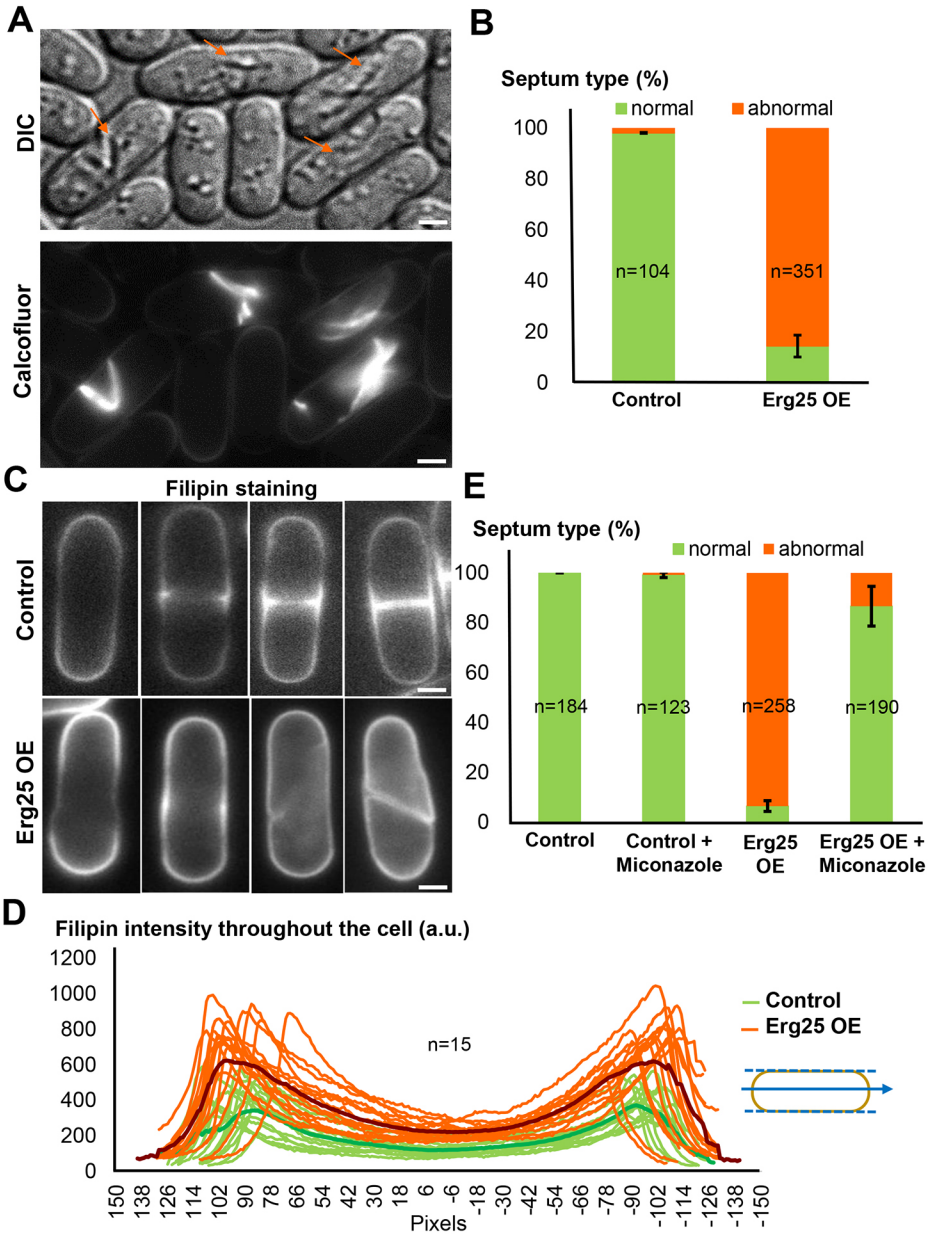

Fig. 1. Erg25 OE induces cytokinesis defect by increasing ergosterol levels. (A) DIC image (top) and Calcofluor staining of septa (bottom) in Erg25 OE cells. Orange arrows indicate cells with abnormal septa. Scale bars: 5 µm. (B) Quantification of the percentage of defective septa in Erg25 OE (n=351) and control cells (n=104). Error bars: s.d. (C) Filipin staining of ergosterol in control (top panel) and Erg25 OE cells (bottom panel). Scale bars: 5 µm. (D) Analysis of filipin intensity along linescans for control (green, n=15) and Erg25 OE cells (orange, n=15). The average curves are displayed in dark green for the control and in dark red for Erg25 OE cells. (E) Quantification of the percentage of defective septa in control or Erg25 OE cells grown in the presence or absence of 1 µM miconazole. Error bars: s.d.

This phenotype was reminiscent of the triple deletion mutant of the reticulon-like proteins Tts1, Rtn1, and Yop1 (hereafter called tryΔ), which displays alteration of the subcortical reticular ER into abnormal cisternae, associated with severe defects in division plane positioning (Zhang et al., 2010). This phenotype has been shown to be suppressed by the deletion of the two vesicle-associated membrane protein-associated proteins (VAPs) genes *scs2* and *scs22*, which link the cortical ER to the plasma membrane. This led to the proposal that abnormal ER cisternae could shield the plasma membrane, preventing normal CR assembly (Zhang et al., 2012). Since Erg25 OE alters ER organization, we wondered if the septum positioning defects it generates could result from the same phenomenon. To test this, Erg25 OE was induced in the VAP single and double deletion mutants. Septum staining with Calcofluor showed that deletion of VAPs only had a minor impact on the effect of Erg25 OE on division plane positioning (~10% reduction in abnormal positioning; Fig. S1G). From this experiment, we conclude that membrane shielding by the ER only has a minor role in the division plane positioning defects produced by Erg25 OE. This result points toward a more direct effect of ergosterol on CR positioning and assembly mechanisms.

To determine how Erg25 OE affects CR assembly, we performed live imaging of Cdr2, the main organizer of cytokinetic precursors, and of Blt1, a component of cytokinetic precursors that remains in the CR until its full constriction (Moseley et al., 2009). These proteins were visualized after fusion to EGFP and mEGFP, respectively, in cells expressing the regulatory light chain of myosin II fused to mCherry (Rlc1–mCherry) in order to follow CR assembly. These cells also expressed the spindle pole body (SPB) component Sid4, also fused to mCherry (Sid4-mCherry), to use SPB separation as a timer for mitosis onset.

Cdr2 was not affected by Erg25 OE (Fig. 2A,B): in cells ranging from 11 to 14 µm in length, neither the length of Cdr2 domain (Fig. S2A) nor the intensity of Cdr2–EGFP were modified (Fig. S2B). Similarly, Blt1 behaved normally during interphase, but at mitotic entry, it started spreading laterally along the cell cortex

Journal of Cell Science (2019) 132, jcs227447. doi:10.1242/jcs.227447

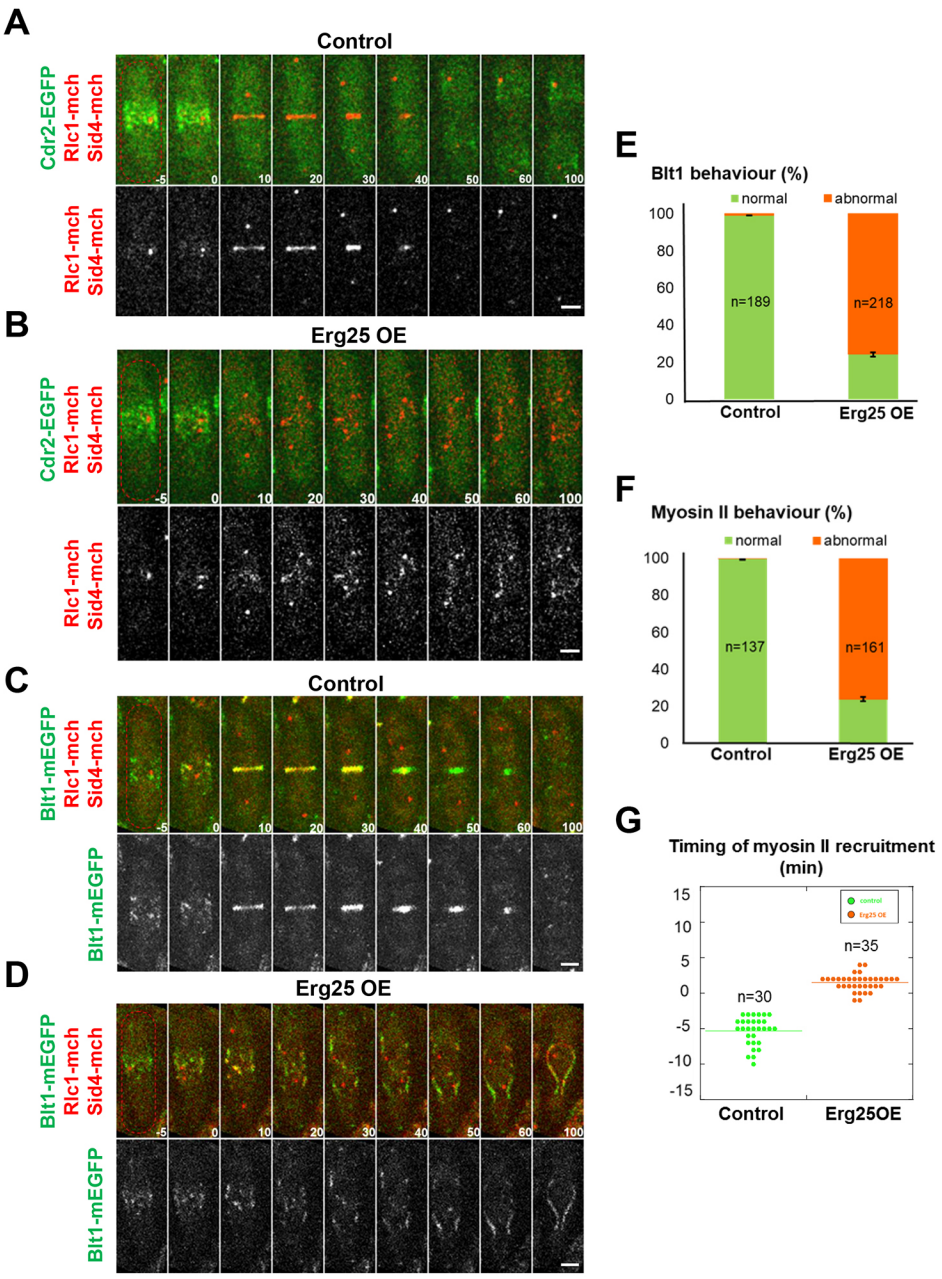

Fig. 2. Erg25 OE affects ring assembly, but not the assembly of cytokinetic precursor nodes in interphase. (A,B) Time-lapse analysis (min) of Cdr2–EGFP, Rlc1–mCherry (mch) and Sid4–mCherry in control (A) and Erg25 OE cells (B) incubated at 25°C for 2 h. Medial plane confocal images are shown. Time 0 corresponds to mitotic entry. (C,D) Time-lapse analysis of Blt1–mEGFP, Rlc1–mCherry and Sid4–mCherry in control (C) and Erg25 OE cells (D) incubated at 25°C for 2 h. Medial plane confocal images are shown. Time 0 corresponds to mitotic entry. Scale bars: 5 µm. (E) Quantification of the percentage of cells where Blt1 showed a normal and abnormal pattern (behaviour) for control (*n*=189) and Erg25 OE cells (*n*=218). (F) Quantification of percentage of cells where myosin II (Rlc1) showed a normal and abnormal pattern (behaviour) for control (*n*=137) and Erg25 OE cells (*n*=161). (G) Timing of myosin II recruitment at cytokinetic precursors after SPB separation (Time 0) in control (*n*=30) and Erg25 OE cells (*n*=35). All error bars represent s.d.

rather than compacting into a ring (Fig. 2C,D). Quantitative analysis showed that 75.7±1.1% (mean±s.d.) of cells overexpressing Erg25 showed an abnormal behaviour of Blt1 in early mitosis compared to 1.0±0.04% in the control situation (Fig. 2E).

We then analysed the behaviour of the light chain of myosin II, Rlc1 in the movies. Although recruited to the medial cortex in early mitosis (Fig. 2A–D; Fig. S3A) to a domain of similar length to that in control cells (2.83±0.23 µm and 2.63±0.18 µm, respectively; Fig. S3B), myosin II was recruited to the cytokinetic precursors with a delay of ∼7 min upon Erg25 OE (Fig. 2G). This delay was confirmed by monitoring the intensity of myosin II in the cell middle (Fig. S3C). While in the control cells, Rlc1–mCherry intensity raised over 30 min before decreasing rapidly at the time of ring constriction, myosin II intensity stopped increasing 20 min after SPB separation in Erg25 OE cells. Intensity then fluctuated at intermediate levels for an extended period of time (Fig. S3C). Strikingly, and similar to Blt1, Rlc1 never compacted into a ring after its recruitment to cytokinetic precursors but spread laterally on the cortex instead (Fig. 2A–D; Fig. S3C, *t*=10 to 20 min). Some abnormal myosin II cables were observed at later time points (Fig. 2A–D; Fig. S3A, *t*=30–100 min). These cables, which ran sometimes along the long axis of the cell, were most often unable to constrict (Fig. 2A,B). Indeed, 76.2±1.1% cells displayed abnormal myosin II rings upon Erg25 OE compared to 0.3±0.4% in the control (Fig. 2F). We conclude that upon Erg25 OE, cytokinetic precursors are well assembled in interphase and competent for myosin II recruitment with a small delay, but they subsequently fail to compact into a ring.

Since the compaction of cytokinetic precursors depends on myosin II-dependent pulling on F-actin filaments nucleated by adjacent nodes (Ojkic et al., 2011; Vavylonis et al., 2008), we next analysed F-actin distribution with Lifeact–GFP (Huang et al., 2012; Riedl et al., 2008). During interphase, Erg25 OE did not alter F-actin patches at the cell tips nor F-actin cables running along the

Journal of Cell Science (2019) 132, jcs227447. doi:10.1242/jcs.227447

length of the cell (Fig. 3A,B). However, after SPB separation, cells failed to accumulate F-actin at the cell middle, indicating that the cytokinetic precursors were unable to promote F-actin assembly upon Erg25 OE (Fig. 3A,B; Fig. S4A,B). Delocalized F-actin dots were detected all over the cell instead, and, after a variable delay, cells started to form F-actin cables with irregular shapes and random orientations [37.0±10.2 min (mean±s.d.) after SPB separation as compared to the appearance of F-actin at the division site 7.3±1.8 min in normal cells; Fig. 3D; see also Movies 1–3]. Quantification revealed that 75.6±1.7% Erg25 OE cells displayed delayed and abnormal F-actin cable assembly compared to 0.6±0.9% in control conditions (Fig. 3C). We conclude that defects in division plane positioning in Erg25 OE cells result from defective F-actin nucleation from cytokinetic precursors.

To understand why F-actin assembly from cytokinetic precursors was abolished in presence of higher ergosterol levels at the medial cortex, we decided to carefully check the whole pathway of recruitment of cytokinetic ring components to cytokinetic precursors (Almonacid et al., 2011; Laporte et al., 2011; Padmanabhan et al., 2011). We started with the anillin-like protein Mid1, which triggers the recruitment of CR ring components to cytokinetic precursors at mitotic onset upon phosphorylation by the polo kinase Plo1 (Almonacid et al., 2011; Bahler et al., 1998a; Celton-Morizur et al., 2004; Paoletti and Chang, 2000; Sohrmann et al., 1996). Similar to Cdr2 and Blt1, and as expected from the fact that myosin II was recruited to medial nodes, Mid1 co-localized normally with Cdr2 at cytokinetic precursors during interphase in Erg25 OE cells (Fig. 4A; Fig. S2C–F). As cells entered mitosis, Mid1 started enriching at the normal timing on the medial cortex upon export from the nucleus (i.e. 2 to 10 min before SPB separation; Fig. 4D) and in a domain of similar length to that of normal cells (Fig. 4E). However, in absence of precursor node compaction, Mid1 then spread along the cell cortex as observed for Blt1 and Rlc1 (Fig. 4A; Fig. S5A).

We next analysed the localization of the IQGAP protein Rng2 (Laporte et al., 2011; Takaine et al., 2014) and of the F-BAR protein Cdc15 (Arasada and Pollard, 2014; Willet et al., 2015a) whose recruitments depend on Mid1. Rng2 and Cdc15 were recruited with

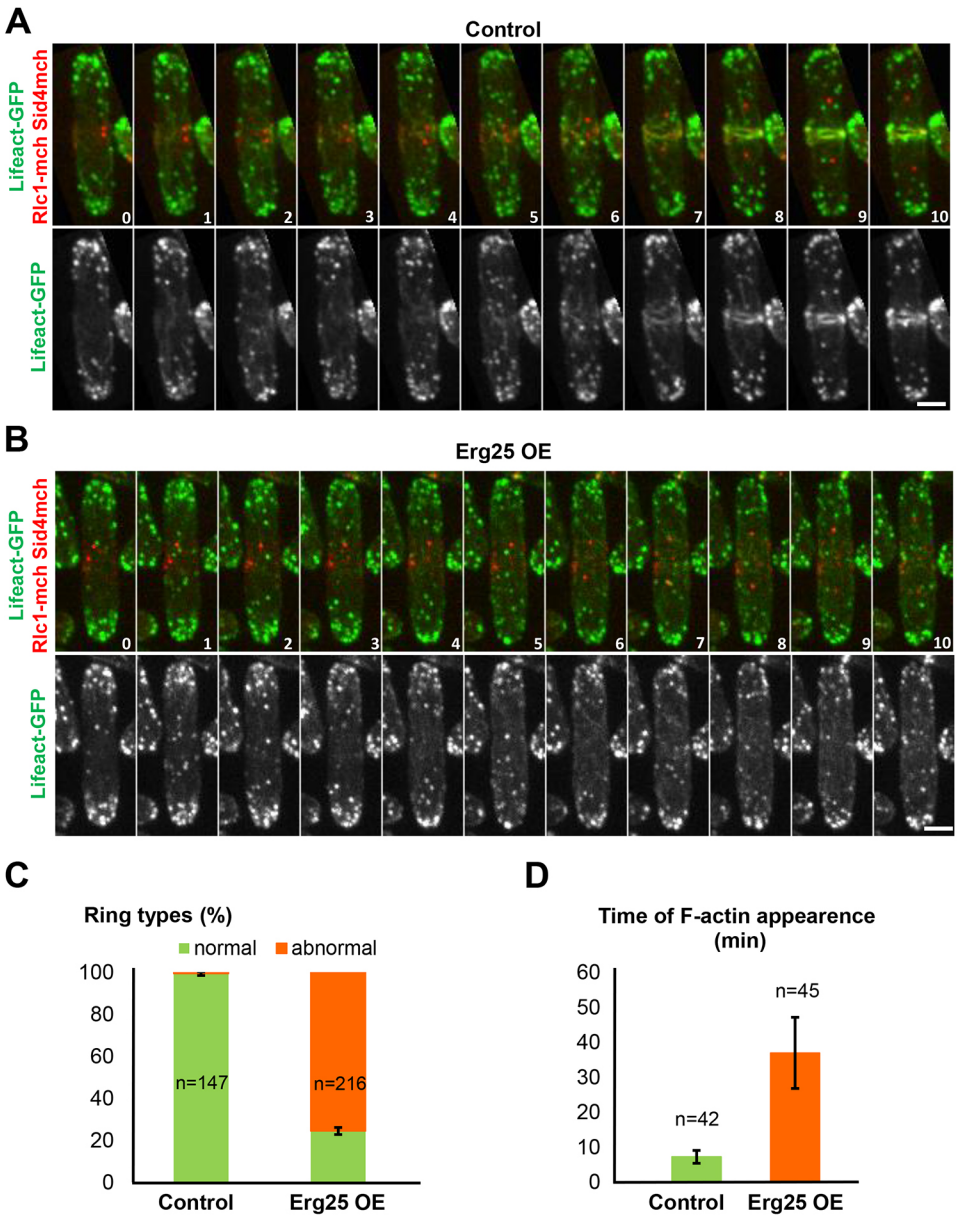

Fig. 3. Inhibition of F-actin nucleation from cytokinetic precursor nodes upon Erg25 OE. Time-lapse imaging (min) of Lifeact–GFP, Rlc1–mCherry (mch) and Sid4–mCherry in control (A) and Erg25 OE cells (B). Maximum projection confocal images are shown. Time 0 corresponds to mitotic entry. Scale bars: 5 µm. (C) Percentage of normal and abnormal contractile rings in control (n=147) and Erg25 OE cells (n=216). Error bars: s.d. (D) Timing of medial actin cable appearance after SPB separation (Time 0) in control (n=42) and Erg25 OE cells (n=45). Error bars: s.d.

Journal of Cell Science (2019) 132, jcs227447. doi:10.1242/jcs.227447

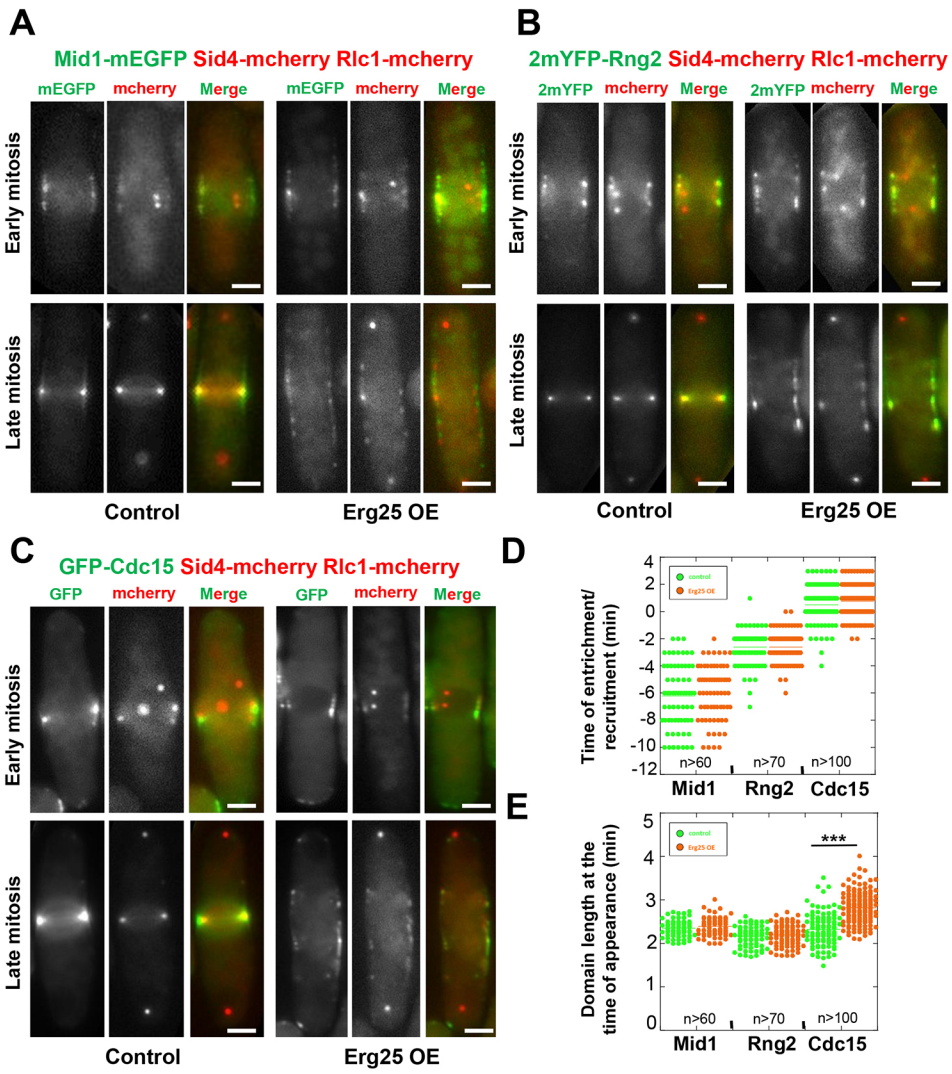

Fig. 4. Erg25 OE does not prevent the recruitment of Mid1, Rng2 and Cdc15 to cytokinetic precursor nodes. (A–C) Epifluorescence images of Mid1–mEGFP (A) or 2mYFP–Rng2 (B) or GFP–Cdc15 (C) and of Rlc1–mCherry and Sid4–mCherry in control and Erg25 OE cells in early mitosis (upper) and late mitosis (bottom). Scale bars: 2 µm. (D) Timing of Mid1 enrichment and Rng2 and Cdc15 recruitment to cytokinetic precursors after SPB separation (time 0) in control (green) and Erg25 OE cells (orange); n>50. (E) Length of Mid1, Rng2 and Cd15 domain at initial time of recruitment in control (green) and Erg25 OE cells (orange); n>50. ***P<0.001.

normal kinetics (Fig. 4B–D) but again, they did not compact into a medial ring and spread out after SPB separation (Fig. 4B,C; Fig. S5B,C). The domain of recruitment was of normal length for Rng2 but slightly enlarged by 0.5 µm for Cdc15 (2.32±0.38 µm in the control and 2.82±1.21 µm upon Erg25 OE, mean±s.d.; Fig. 4E). Since Cdc15 is recruited a few minutes later than Rlc1 or Rng2, the expansion of the domain of recruitment might be due to the spreading of cytokinetic precursors observed during the course of mitosis in Erg25 OE cells.

We finally examined the formin Cdc12, which is responsible for F-actin nucleation from cytokinetic precursors. Cdc12 recruitment depends on the recruitment of all other components of the CR mentioned above (Laporte et al., 2011). Although the Cdc12 signal in fusion to either three YFP tags or three GFP tags was very faint, we were able to detect its recruitment to cytokinetic precursors in all cells examined (Fig. 5A,D,E) and to establish that there was no alteration in the timing of its recruitment upon Erg25 OE (7.38±1.85 min in the control and 7.22±1.95 min upon Erg25 OE; Fig. 5B). But Cdc12 was recruited to a larger domain (2.19±0.19 µm in Erg25 OE cells compared to 0.96±0.12 µm in control cells; Fig. 5C). The enlargement of the domain could be due to precursor node spreading over the cortex upon Erg25 OE instead of compacting as soon as Cdc12 is recruited and promotes F-actin assembly.

Given the weak signals observed for Cdc12, we also designed a control experiment to ascertain that the faint signals observed were genuine: *cdc25-22* cells overexpressing Erg25 synchronized by block in G2 for 2 h at 36°C and released into mitosis at 25°C were compared to *cdc25-22* cells and to *mid1*Δ *cdc25-22* cells, which cannot recruit Cdc12 on medial cortex in mitosis (Laporte et al., 2011). While no signal was detected in *mid1*Δ cells, Erg25 OE cells showed faint Cdc12 nodes dispersed along the medial cell cortex upon Erg25 OE (Fig. 5F).

Unfortunately, the low signal of Cdc12, and its dispersion on the medial cortex upon Erg25 OE prevented us from quantifying the amounts of Cdc12 recruited to cytokinetic precursors. Therefore, although we can confirm that Cdc12 is still recruited to cytokinetic precursors upon Erg25 OE, we cannot exclude quantitative defects in Cdc12 recruitment in Erg25 OE cells at this stage. In any case, since F-actin assembly is fully abolished, we conclude that the molecules of Cdc12 recruited to cytokinetic precursors are unable to induce the assembly of stable F-actin cables.

We next wondered whether Erg25 OE could result in a general defect of F-actin cable stability or assembly by formins. To assess whether this was the case, we analysed F-actin distribution in interphase cells, in which F-actin cable formation depends exclusively on the formin For3 (Feierbach and Chang, 2001). Interphase cells overexpressing Erg25 presented normal For3-nucleated F-actin

Journal of Cell Science (2019) 132, jcs227447. doi:10.1242/jcs.227447

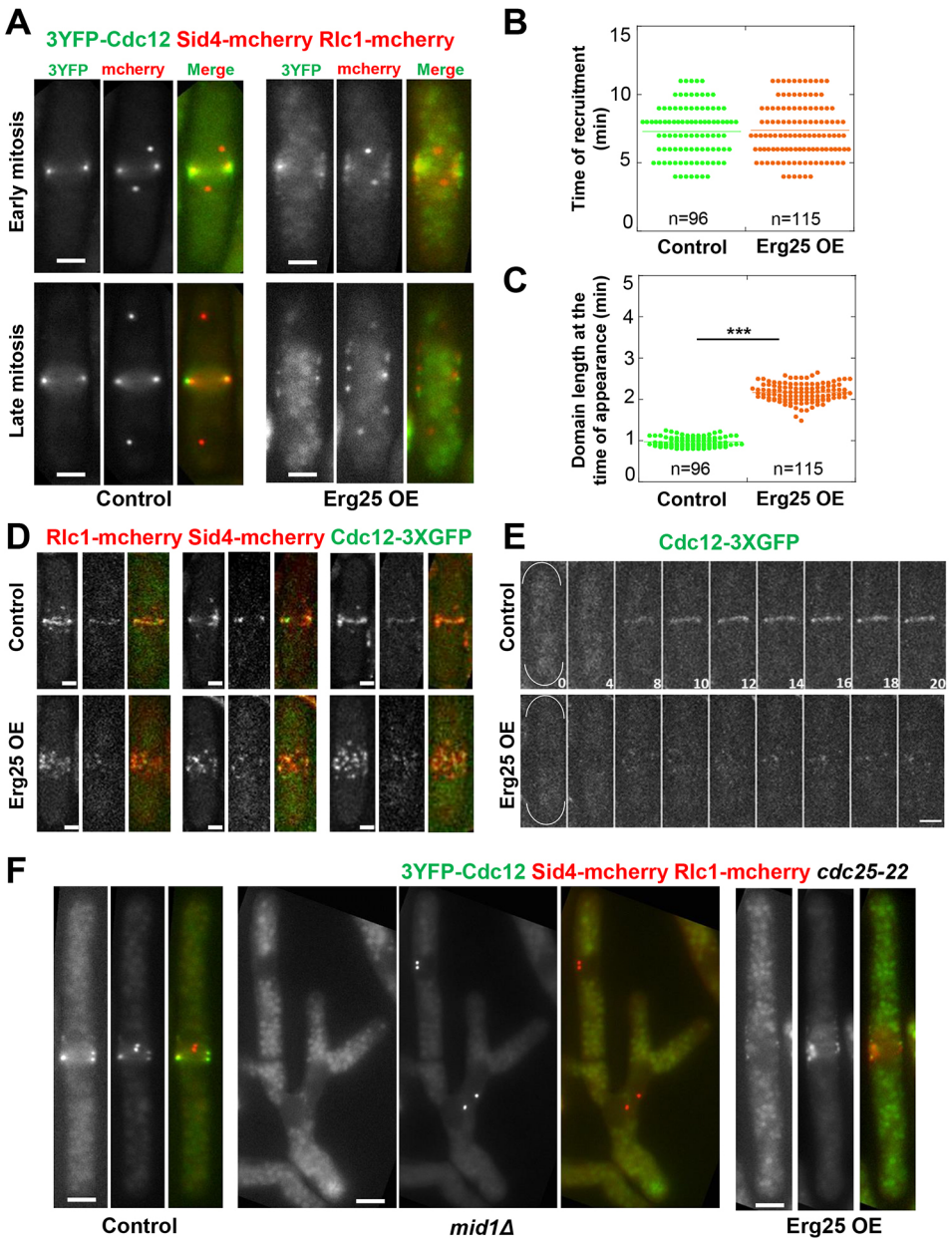

Fig. 5. Erg25 OE does not prevent the recruitment of the formin Cdc12 to cytokinetic precursor nodes. (A) Epifluorescence medial plane images of 3YFP–Cdc12, Rlc1–mCherry and Sid4–mCherry in control and Erg25 OE cells in early mitosis (upper) and late mitosis (bottom). Scale bars: 5 µm. (B) Timing of Cdc12–3×GFP recruitment to cytokinetic precursor nodes after SPB separation (time 0) in control (green, *n*=96) and Erg25 OE cells (orange, *n*=115). (C) Length of the Cdc12–3×GFP domain at initial time of recruitment in control (green, *n*=96) and Erg25 OE cells (orange, *n*=115). ***$P<10^{-10}$. (D) Maximum projections of confocal *z*-stacks showing the Cdc12–3×GFP, Rlc1–mCherry and Sid4–mCherry distribution in control (top) and Erg25 OE cells (bottom). Scale bars: 2 µm. (E) Time lapse images (min) of Cdc12–3×GFP in control (top) and Erg25 OE cells (bottom). Time 0 corresponds to the time of SPB separation. Scale bar: 5 µm. (F) Epifluorescence images of 3YFP–Cdc12, Rlc1–mCherry and Sid4–mCherry at the time of SPB separation in synchronized *cdc25-22* control (left), *mid1Δ* (center) and Erg25 OE cells (right). Scale bars: 5 µm.

cables, and quantitative analysis did not reveal a reduction in the mean number of F-actin cables per cell (Fig. 6A,B). This implies that F-actin cable assembly and stability are not impaired altogether in Erg25 OE cells, and that the formin For3 but also the profilin Cdc3 and the tropomyosin Cdc8, which are necessary for For3-dependent F-actin cable assembly (Balasubramanian et al., 1992, 1994), are not affected by increased ergosterol levels. This suggest that increased ergosterol levels may specifically inhibit the function of the mitotic formin Cdc12.

Since the assembly of F-actin cables by Cdc12 was shown to be in competition with the assembly of actin patches mediated by the Arp2/3 complex (Suarez et al., 2015), we further tested whether Cdc12 inhibition was responsible for Erg25 OE effects by blocking Arp2/3 function in Erg25 overexpressing cells with CK666, reasoning that it should rescue CR assembly. CK666 treatment was performed in cells expressing Lifeact–GFP as well as Rlc1–mCherry and Sid4–mCherry. In wild-type and Erg25 OE cells in interphase, we first observed as expected a fast disappearance of F-actin patches, and an accumulation of For3-dependent F-actin cables (Fig. 6A). Next, by looking at cells overexpressing Erg25 entering mitosis within 1 h of CK666 treatment, we observed an increase in the number of medially placed contractile rings as compared to what was seen in non-treated cells overexpressing Erg25 (Fig. 6C). This indicates that Arp2/3 inhibition can rescue the effect of Erg25 OE. Since Arp2/3 complex inhibition affects endocytosis, which may in turn alter membrane composition, we also verified ergosterol levels before and after CK666 treatment. While a mild reduction of ergosterol levels was detected in the control, high ergosterol levels were maintained 1 h after CK666 addition in Erg25 OE cells (Fig. S6). This rules out the possibility that the partial suppression of the Erg25 OE phenotype upon CK666 treatment is due to a reduction in the ergosterol amounts. Rather, by favouring actin availability for formin, due to the inhibition of Arp2/3, there is a partial rescue in the ability of Erg25 OE cells to assemble F-actin from cytokinetic precursors. Likewise, a small reduction in the number of abnormally placed contractile rings was

Journal of Cell Science (2019) 132, jcs227447. doi:10.1242/jcs.227447

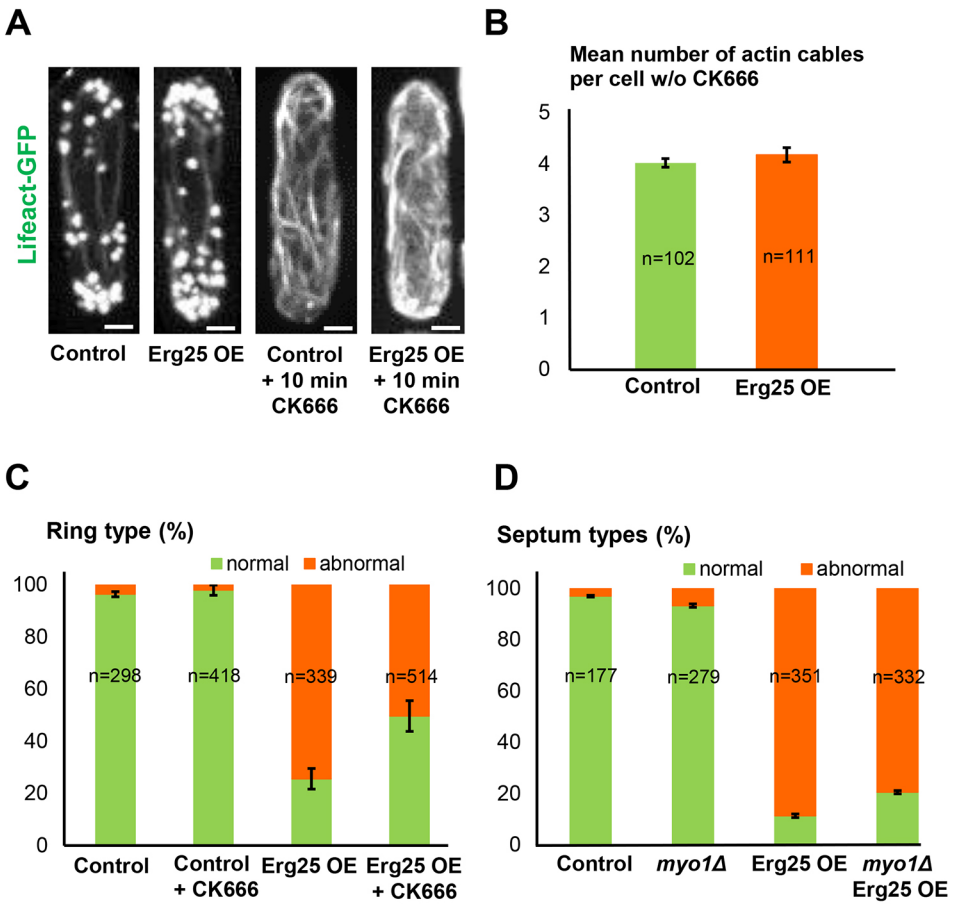

Fig. 6. Inhibition of the Arp2/3 complex by CK666 partially rescues the effects of Erg25 OE. (A) Lifeact–GFP fluorescence in control and Erg25 OE cells, 10 min after being treated or not with CK666. Maximum intensity projections of *z*-series acquired at 0.3 µm intervals. Scale bars: 5 µm. (B) Mean number of F-actin cables per interphase cell measured from maximum intensity projections in wild-type (*n*=102) and Erg25 OE cells (*n*=111). (C) Percentage of normal and abnormal rings assembled within 1 h after the addition or not of 100 µM CK666, as measured in time-lapse movies of control (*n*=298 w/o CK666 and *n*=418 with CK666) and Erg25 OE cells (*n*=339 w/o CK666 and *n*=514 with CK666). (D) Quantification of the percentage of normal and abnormal septum types as determined through Calcofluor staining in wild-type (*n*=177), Erg25 OE (*n*=279), *myo1Δ* (*n*=351) and Erg25 OE *myo1Δ* cells (*n*=332). All error bars represent s.d.

observed in the deletion mutant of Myo1 (Myo1 is known to act as an activator of Arp2/3 and also to organize sterol-rich domains) (Fig. 6D) (Lee et al., 2000; Sirotkin et al., 2005; Takeda and Chang, 2005). These experiments are in agreement with our hypothesis that increased ergosterol levels may inhibit the Cdc12-dependent assembly of F-actin cables from cytokinetic precursors.

DISCUSSION

Although Erg25 OE results in a similar phenotype to that seen upon the absence of the anillin-like protein Mid1, which blocks the recruitment of essential CR components to cytokinetic precursors, and that seen upon the deletion of reticulon-like proteins (tryΔ mutant), which transforms the subcortical reticular ER into cisternae, strikingly enough, neither of these pathways seems to be strongly affected by Erg25 OE.

Our results show that Erg25 OE results in a moderate delay in myosin II recruitment. Since neither Mid1 accumulation in medial nodes upon nuclear export, nor Rng2 recruitment were delayed, we can exclude that this results from a defect in Mid1 activation by Plo1 (Almonacid et al., 2011; Padmanabhan et al., 2011; Laporte et al., 2011). One hypothesis to explain this delay is that increasing ergosterol levels may create a lipid environment that alters the ability of myosin II to interact with Rng2.

Nevertheless, this short delay in myosin II recruitment cannot account for the strong division plane positioning defects. Accordingly, we observed another major phenotype upon Erg25 OE, consisting of an inhibition of Cdc12-dependent F-actin assembly from cytokinetic precursors in early mitosis. While we cannot exclude a reduction in the amounts recruited to cytokinetic precursors, the formin Cdc12 was always recruited to cytokinetic nodes at the proper time, i.e. ∼7 min after mitotic entry. However, cytokinetic precursors did not generate F-actin filaments. Importantly, analysing F-actin cables generated by the formin For3 during interphase ruled out a general effect of Erg25 OE on F-actin cable stability or on formins in general. Furthermore, the phenotype produced by increased ergosterol levels was partially rescued by inhibiting Arp2/3, which competes with the formin Cdc12 (Suarez et al., 2015). Taken together, these data suggest that high ergosterol levels may directly or indirectly affect the activity of the formin Cdc12.

In contrast to what is observed in *cdc12* mutants that only display randomly organized medial wisps of actin that are not able to condense into a ring structure (Chang et al., 1997, 1996), Erg25 overexpressing cells sometimes managed to assemble misshapen and mis-oriented contractile rings after a long delay, ranging from 20 to 40 min. This suggests that Erg25 OE may affect Cdc12 activity only transiently or partially, or that in late stages of cytokinesis, an activatory mechanism for Cdc12 can overcome the inhibition imposed on Cdc12 by increased ergosterol levels.

Cdc12 is an atypical formin that is not regulated by Rho-type GTPases or an auto-inhibitory domain (Yonetani et al., 2008; Bohnert et al., 2013). However, Cdc12 hyperactivity is lethal (Kovar et al., 2003), indicating that its function needs to be strictly controlled. Cdc12 is also subject to SIN-dependent regulation; the kinase Sid2 inhibits Cdc12 multimerization in order to properly assemble and maintain the CR (Bohnert et al., 2013; Willet et al., 2015b). Our results suggest that the lipid environment of Cdc12 at the plasma membrane could represent a novel mechanism to negatively regulate Cdc12 activity, and possibly also its level of recruitment.

How could the lipid composition of the plasma membrane regulate the activity of a formin? Previous work has revealed that the

localization and activity of the mammalian formin mDia1 is tuned by interactions with phospholipids (Ramalingam et al., 2010). This multidomain protein is able to bind to negatively charged phospholipids (PIP_2 and phosphatidylserine) through a basic domain located in the N-terminus of the protein, which mediates its recruitment at the plasma membrane, and an additional membrane-binding site in the C-terminal region has been shown to inhibit mDia1 F-actin polymerization activity (Ramalingam et al., 2010). This shows that the recruitment and the activation of formins are two distinct processes and that lipids can play an active role in both processes. Our results in fission yeast suggest that ergosterol levels may exert an inhibitory effect on Cdc12 by affecting its F-actin nucleation activity and possibly, its full recruitment to the cortex.

From the point of view of the PM composition homeostasis, it is legitimate to wonder whether increased levels of ergosterols have an impact in the composition or organization of other plasma membrane lipids. Indeed, ergosterols preferentially sort to the outer leaflet of the plasma membrane (Solanko et al., 2018), and their overproduction may affect the distribution of other membrane components on the inner leaflet of the plasma membrane. As mentioned above, PIP_2 plays important roles in cytokinesis. In our experiments using the PH domain of PLC1δ as a molecular probe for PIP_2, no major changes of this phospholipid could be detected upon Erg25 OE at the moment of ring assembly (our unpublished results). Although we cannot exclude the possibility that other lipids might affect cytokinesis, we favour the hypothesis that the defective ring assembly produced upon Erg25 OE is likely to be due to increased ergosterol levels per se.

Furthermore, tight-packed sphingolipid–sterol clusters prime lipid–lipid and lipid–protein interactions by sorting them according to their length and level of saturation (Simons and Ikonen, 1997; Simons and Toomre, 2000). In this way, SRDs organize the plasma membrane in dynamic microdomains that, by concentrating specific groups of proteins, can contribute to membrane and cytoskeleton changes. Strikingly, the F-BAR protein Cdc15 is both involved in the regulation of Cdc12 (Bohnert et al., 2013) and in the organization of a SRD at the division site in late cytokinesis (Takeda et al., 2004). This makes of Cdc15 a good candidate to link Cdc12 regulation to sterol concentration. Further work will then be necessary to determine whether and how Cdc15 could be involved in this process.

Finally, the physiological relevance of the negative regulation of cytokinetic F-actin cables assembly by ergosterol levels remains to be defined.

To conclude, we have shown that ergosterol levels at the plasma membrane can regulate Cdc12-dependent assembly of F-actin cables from cytokinetic precursors, a crucial step for the assembly of the cytokinetic ring. The molecular mechanisms by which ergosterol levels might regulate Cdc12 remain elusive at this stage. An interesting approach would be to turn to *in vitro* studies in presence of lipids to determine whether membrane lipids can directly influence Cdc12 activity. This would help us to understand the impact of membrane microenvironment on CR assembly. It will also be very interesting to determine whether our finding are relevant to animal cells, where formins play a key role in cytokinesis, and in other cellular processes where SRDs are also involved such as cell polarity or cell migration (Gomez-Mouton et al., 2001; Head et al., 2014; Mañes et al., 1999; Seveau et al., 2001).

MATERIALS AND METHODS

Strains and plasmids

Standard *S. pombe* media and genetic manipulations were used. All strains used in the study were isogenic to wild-type 972 and are described in Table S1. Strains from genetic crosses were selected by random spore germination and replica in plates with appropriate supplements or drugs.

For *erg25* overexpression, the plasmid pAF12, a derivative of pREP3x (Maundrell, 1993) was created by cloning the *erg25* open reading frame (ORF) between the SalI and BamHI sites of the vector polylinker. In parallel, we created pAF23, a modified pREP42X plasmid (Basi et al., 1993) in which the weaker *nmt1* promoter of pREP42X was replaced by the strongest *nmt1* promoter, by cloning it between SacI and PstI sites, upstream of the *erg25* ORF. All plasmids were checked by diagnostic PCR and restriction enzyme digestion, and the DNA fragments amplified by PCR were sequenced.

The *erg6*, *scs2* and *scs22* genes were deleted according to the method described in Bahler et al. (1998b). KanMX6- or NatMX6-resistant transformants were checked by PCR for correct DNA integration in the desired locus.

Transformations were performed by using the lithium-DTT method. 20 ml of exponentially growing cells [optical density at 600 nm (OD_{600}) of 0.5–0.8] were harvested by centrifugation (2500 ***g*** for 5 min) and washed with 10 mM Tris-HCl pH 7.4. After a second centrifugation (600 ***g*** for 1 min), they were re-suspended in 100 mM lithium acetate with 10 mM DTT and were incubated on an orbital wheel at room temperature for 40 min. 100 µl of these cells were mixed with 80 µl of 100 mM lithium acetate, 10 µl of single-stranded DNA from salmon testes (D9156-5ML, Sigma-Aldrich) and 2 µg of the desired plasmid or the purified PCR product. After 10 min of incubation on an orbital wheel, 300 µl of PEG 4000, previously diluted 1:1 in 100 mM lithium acetate, was added. After a second round of 10 min on the wheel, 15 µl of DMSO were added and the cells were subjected to heat shock at 42°C for 20 min in a water bath. Cells were then plated on selection plates. To induce Erg25 OE, cells were grown overnight at 25°C in EMM2S with 0.5 µg/ml thiamine. The following day, cells were washed three times with sterile water and were inoculated in EMM2S without thiamine for 24 h.

Live-cell imaging and microscopy

Epifluorescence images were taken on a DMRXA2 upright microscope (Leica Microsystems), equipped with a 100×1.4NA oil immersion PlanApo objective and a Coolsnap HQ CCD camera (Photometrics). Exposure times were 2 s for GFP, 1 s for mCherry and 10 ms for Calcofluor or filipin staining. To analyse Erg25–ENVY localization an exposure time of 500 ms for GFP was used.

To measure filipin intensity, a linescan throughout cells ranging from 11.5 to 13.5 µm in length was drawn according to the scheme shown in Fig. 1D.

For time-lapse imaging, 1 ml of exponentially growing cells were harvested by centrifugation (600 ***g*** for 1 min), the supernatant was discarded and 1 µl of the cells was deposited in a 2% YE5S agar pad at the center of PDMS slide chambers prepared as described in (Costa et al., 2013).

Time-lapse movies were acquired with an inverted Spinning Disc Confocal (Roper/Nikon), equipped with a Plan Apochromat 100×1.4 NA objective lens (Nikon), a PIFOC (perfect image focus) objective stepper, and a charge-coupled device camera (EMCCD 512×512 QuantEM; Photometrics). To analyse Cdr2–EGFP, Blt1–mEGFP, GFP–Cdc15 and F-actin, stacks of seven planes spaced at 1 µm apart were acquired every 1 min for 3 h (binning 1, 300 EM gain; 200 ms exposure with 6% laser power for GFP and 5.5% laser power for mCherry). For analysis of recruitment/enrichment of Mid1–mEGFP, 2mYFP–Rng2 and Cdc12–3XGFP similar movies of 1 h were acquired with a laser power of 8% for GFP.

All images were acquired and processed with MetaMorph 7.8 (Molecular Devices).

Analysis of the Cdr2–EGFP domain length was performed on single medial planes of images acquired with a spinning disc confocal microscope with 2 s exposure of 7% GFP laser power. The fluorescence intensity of Cdr2–EGFP was measured on maximal projections of *z*-stacks of seven planes spaced at 1 µm apart on a 40-pixel-long line along the medial cortex. Background fluorescence measured at the cell tips was then deduced.

To determine the Mid1–mEGFP and Cdr2–tagRFP cortical fluorescence intensity, stacks of seven planes spaced at 1µm apart were acquired (binning 1, 300 EM gain; 2 s exposure with 7% laser power for GFP and 7% laser power for mCherry). Intensity along a 100-pixel-long line on the medial cortex was measured on single medial focal planes taken with a spinning

disc confocal microscope. The percentage of Cdr2 nodes containing Mid1 was derived from linescans as the percentage of Cdr2 peaks corresponding to a Mid1 peak.

For myosin II intensity measurement, the strain containing Rlc1–mCherry and Sid4–GFP was imaged with a spinning disc confocal microscope, and stacks of seven planes spaced at 1 µm apart was acquired every 1 min for 3 h (binning 1, 300 EM gain; 100 ms exposure with 10% laser power for GFP and 5.5% laser power for mCherry). The Rlc1–mCherry signal was measured on maximal projection of 3D-stacks in a rectangle in the cell middle (scheme in Fig. S4C). Background measured at the cell tips was then deduced.

Calcofluor staining

Cell wall staining was performed by mixing 1 ml of early exponentially growing cells with 5 µl of 10 mg/ml Calcofluor (Fluorescent Brightener 28, F3543, Sigma). After washing the cells in 1 ml of PBS, 2 µl of the mix was deposited on slides for microscopy.

Miconazole treatment

Control and Erg25 OE cells were grown overnight in EMM2S with 15 µM thiamine to achieve exponential growth. Cells were washed three times with water and inoculated in EMM2S without thiamine to induce Erg25 OE for 22 h in the presence or absence of miconazole 1 µM before analysing septum morphology through Calcofluor staining.

Filipin staining

Filipin (F4767, Sigma-Aldrich) was dissolved in DMSO to create a stock at 5 mg/ml. Sterol staining was performed by adding 5 µl of the filipin stock to 1 ml of cell culture, and cells were observed immediately to avoid filipin internalization (Wachtler et al., 2003).

CK666 treatment

CK666 (SML0006, Sigma-Aldrich) was used at the final concentration of 100 µM from a 500× stock dissolved in DMSO. Cells with Lifeact–GFP marker were incubated with the drug and immediately imaged for 1 h with a spinning disc confocal microscopy (*z*-stacks of seven planes spaced by 1 µm were acquired every 1 min, binning 1, 300 EM gain; 200 ms exposure with 6% laser power for GFP and 5.5% laser power for mCherry).

The number of actin cables in interphase cells of 10.5 to 12.5 µm in length was measured 10 min after CK666 treatment from maximum intensity projections of confocal z-stack spanning the entire cell at 0.3 µm intervals (binning 1, 100 EM gain, 500 ms exposure with 25.5% laser power for GFP).

Statistical analysis

Sample size (*n*) is defined in each figure and is derived from three independent experiments. The error bars correspond to standard deviation (s.d.) between experiments and are specifically indicated in each figure. Throughout all figures, two-tailed *t*-test analysis on homoscedastic populations were applied: the significance of this statistical test is marked with asterisks, with $*P<0.05$, $**P<0.01$ and $***P<0.001$.

Acknowledgements

We thank Vincent Fraisier for maintenance of the microscope setups that were used in this study. Imaging was performed at PICT-IBISA (Institut Curie, Paris) which is part of France-Bioimaging national research infrastructure.

Competing interests

The authors declare no competing or financial interests.

Author contributions

Conceptualization: S.A.R., A.P.; Methodology: F.A., S.A.R., A.P.; Software: F.A.; Validation: F.A., S.A.R., A.P.; Formal analysis: F.A.; Investigation: F.A.; Resources: S.A.R., A.P.; Data curation: F.A.; Writing - original draft: F.A., S.A.R., A.P.; Writing - review & editing: S.A.R., A.P.; Visualization: F.A.; Supervision: S.A.R., A.P.; Project administration: S.A.R., A.P.; Funding acquisition: F.A.

Funding

This work was supported by a grant from Fondation ARC pour la Recherche sur le Cancer (PJA 20171206550) to A.P., which also provided a. received a fourth year PhD fellowship to F.A. A.P. is a member of the LabEx CelTisPhyBio.

Supplementary information

Supplementary information available online at
http://jcs.biologists.org/lookup/doi/10.1242/jcs.227447.supplemental

References

Akamatsu, M., Berro, J., Pu, K.-M., Tebbs, I. R. and Pollard, T. D. (2014). Cytokinetic nodes in fission yeast arise from two distinct types of nodes that merge during interphase. *J. Cell Biol.* **204**, 977-988. doi:10.1083/jcb.201307174

Akamatsu, M., Lin, Y., Bewersdorf, J. and Pollard, T. D. (2017). Analysis of interphase node proteins in fission yeast by quantitative and superresolution fluorescence microscopy. *Mol. Biol. Cell* **28**, 3203-3214. doi:10.1091/mbc.e16-07-0522

Almonacid, M., Moseley, J. B., Janvore, J., Mayeux, A., Fraisier, V., Nurse, P. and Paoletti, A. (2009). Spatial control of cytokinesis by Cdr2 kinase and Mid1/anillin nuclear export. *Curr. Biol.* **19**, 961-966. doi:10.1016/j.cub.2009.04.024

Almonacid, M., Celton-Morizur, S., Jakubowski, J. L., Dingli, F., Loew, D., Mayeux, A., Chen, J.-S., Gould, K. L., Clifford, D. M. and Paoletti, A. (2011). Temporal control of contractile ring assembly by Plo1 regulation of myosin II recruitment by Mid1/anillin. *Curr. Biol.* **21**, 473-479. doi:10.1016/j.cub.2011.02.003

Alvarez, F. J., Douglas, L. M. and Konopka, J. B. (2007). Sterol-rich plasma membrane domains in fungi. *Eukaryot. Cell* **6**, 755-763. doi:10.1128/EC.00008-07

Arasada, R. and Pollard, T. D. (2014). Contractile ring stability in S. pombe depends on F-BAR protein Cdc15p and Bgs1p transport from the Golgi complex. *Cell Rep* **8**, 1533-1544. doi:10.1016/j.celrep.2014.07.048

Atilla-Gokcumen, G. E., Muro, E., Relat-Goberna, J., Sasse, S., Bedigian, A., Coughlin, M. L., Garcia-Manyes, S. and Eggert, U. S. (2014). Dividing cells regulate their lipid composition and localization. *Cell* **156**, 428-439. doi:10.1016/j.cell.2013.12.015

Bahler, J., Steever, A. B., Wheatley, S., Wang, Y., Pringle, J. R., Gould, K. L. and McCollum, D. (1998a). Role of polo kinase and Mid1p in determining the site of cell division in fission yeast. *J. Cell Biol.* **143**, 1603-1616. doi:10.1083/jcb.143.6.1603

Bahler, J., Wu, J. Q., Longtine, M. S., Shah, N. G., McKenzie, A., III, Steever, A. B., Wach, A., Philippsen, P. and Pringle, J. R. (1998b). Heterologous modules for efficient and versatile PCR-based gene targeting in Schizosaccharomyces pombe. *Yeast* **14**, 943-951. doi:10.1002/(SICI)1097-0061(199807)14:10<943::AID-YEA292>3.0.CO;2-Y

Baird, D., Stefan, C., Audhya, A., Weys, S. and Emr, S. D. (2008). Assembly of the PtdIns 4-kinase Stt4 complex at the plasma membrane requires Ypp1 and Efr3. *J. Cell Biol.* **183**, 1061-1074. doi:10.1083/jcb.200804003

Balasubramanian, M. K., Helfman, D. M. and Hemmingsen, S. M. (1992). A new tropomyosin essential for cytokinesis in the fission yeast S. pombe. *Nature* **360**, 84-87. doi:10.1038/360084a0

Balasubramanian, M. K., Hirani, B. R., Burke, J. D. and Gould, K. L. (1994). The Schizosaccharomyces pombe cdc3+ gene encodes a profilin essential for cytokinesis. *J. Cell Biol.* **125**, 1289-1301. doi:10.1083/jcb.125.6.1289

Bard, M., Bruner, D. A., Pierson, C. A., Lees, N. D., Biermann, B., Frye, L., Koegel, C. and Barbuch, R. (1996). Cloning and characterization of ERG25, the Saccharomyces cerevisiae gene encoding C-4 sterol methyl oxidase. *Proc. Natl. Acad. Sci. USA* **93**, 186-190. doi:10.1073/pnas.93.1.186

Basi, G., Schmid, E. and Maundrell, K. (1993). TATA box mutations in the Schizosaccharomyces pombe nmt1 promoter affect transcription efficiency but not the transcription start point or thiamine repressibility. *Gene* **123**, 131-136. doi:10.1016/0378-1119(93)90552-E

Bohnert, K. A., Grzegorzewska, A. P., Willet, A. H., Vander Kooi, C. W., Kovar, D. R. and Gould, K. L. (2013). SIN-dependent phosphoinhibition of formin multimerization controls fission yeast cytokinesis. *Genes Dev.* **27**, 2164-2177. doi:10.1101/gad.224154.113

Carnahan, R. H. and Gould, K. L. (2003). The PCH family protein, Cdc15p, recruits two F-actin nucleation pathways to coordinate cytokinetic actin ring formation in Schizosaccharomyces pombe. *J. Cell Biol.* **162**, 851-862. doi:10.1083/jcb.200305012

Cauvin, C. and Echard, A. (2015). Phosphoinositides: lipids with informative heads and mastermind functions in cell division. *Biochim. Biophys. Acta* **1851**, 832-843. doi:10.1016/j.bbalip.2014.10.013

Celton-Morizur, S., Bordes, N., Fraisier, V., Tran, P. T. and Paoletti, A. (2004). C-terminal anchoring of mid1p to membranes stabilizes cytokinetic ring position in early mitosis in fission yeast. *Mol. Cell. Biol.* **24**, 10621-10635. doi:10.1128/MCB.24.24.10621-10635.2004

Celton-Morizur, S., Racine, V., Sibarita, J.-B. and Paoletti, A. (2006). Pom1 kinase links division plane position to cell polarity by regulating Mid1p cortical distribution. *J. Cell Sci.* **119**, 4710-4718. doi:10.1242/jcs.03261

Chang, F., Woollard, A. and Nurse, P. (1996). Isolation and characterization of fission yeast mutants defective in the assembly and placement of the contractile actin ring. *J. Cell Sci.* **109**, 131-142.

Chang, F., Drubin, D. and Nurse, P. (1997). cdc12p, a protein required for cytokinesis in fission yeast, is a component of the cell division ring and interacts with profilin. *J. Cell Biol.* **137**, 169-182. doi:10.1083/jcb.137.1.169

Coffman, V. C., Nile, A. H., Lee, I.-J., Liu, H. and Wu, J.-Q. (2009). Roles of formin nodes and myosin motor activity in Mid1p-dependent contractile-ring assembly during fission yeast cytokinesis. *Mol. Biol. Cell* **20**, 5195-5210. doi:10.1091/mbc.e09-05-0428

Coffman, V. C., Sees, J. A., Kovar, D. R. and Wu, J.-Q. (2013). The formins Cdc12 and For3 cooperate during contractile ring assembly in cytokinesis. *J. Cell Biol.* **203**, 101-114. doi:10.1083/jcb.201305022

Costa, J., Fu, C., Syrovatkina, V. and Tran, P. T. (2013). Imaging individual spindle microtubule dynamics in fission yeast. *Methods Cell Biol.* **115**, 385-394. doi:10.1016/B978-0-12-407757-7.00024-4

Dambournet, D., Machicoane, M., Chesneau, L., Sachse, M., Rocancourt, M., El Marjou, A., Formstecher, E., Salomon, R., Goud, B. and Echard, A. (2011). Rab35 GTPase and OCRL phosphatase remodel lipids and F-actin for successful cytokinesis. *Nat. Cell Biol.* **13**, 981-988. doi:10.1038/ncb2279

Echard, A. (2012). Phosphoinositides and cytokinesis: the "PIP" of the iceberg. *Cytoskeleton* **69**, 893-912. doi:10.1002/cm.21067

Echard, A. and Burgess, D. (2014). The changing lipidome during cell division. *Cell* **156**, 394-395. doi:10.1016/j.cell.2014.01.018

Feierbach, B. and Chang, F. (2001). Roles of the fission yeast formin for3p in cell polarity, actin cable formation and symmetric cell division. *Curr. Biol.* **11**, 1656-1665. doi:10.1016/S0960-9822(01)00525-5

Feoktistova, A., Magnelli, P., Abeijon, C., Perez, P., Lester, R. L., Dickson, R. C. and Gould, K. L. (2001). Coordination between fission yeast glucan formation and growth requires a sphingolipase activity. *Genetics* **158**, 1397-1411.

Fujiwara, T., Bandi, M., Nitta, M., Ivanova, E. V., Bronson, R. T. and Pellman, D. (2005). Cytokinesis failure generating tetraploids promotes tumorigenesis in p53-null cells. *Nature* **437**, 1043-1047. doi:10.1038/nature04217

Gomez-Mouton, C., Abad, J. L., Mira, E., Lacalle, R. A., Gallardo, E., Jimenez-Baranda, S., Illa, I., Bernad, A., Manes, S. and Martinez-A, C. (2001). Segregation of leading-edge and uropod components into specific lipid rafts during T cell polarization. *Proc. Natl. Acad. Sci. USA* **98**, 9642-9647. doi:10.1073/pnas.171160298

Goss, J. W., Kim, S., Bledsoe, H. and Pollard, T. D. (2014). Characterization of the roles of Blt1p in fission yeast cytokinesis. *Mol. Biol. Cell* **25**, 1946-1957. doi:10.1091/mbc.e13-06-0300

Guzman-Vendrell, M., Baldissard, S., Almonacid, M., Mayeux, A., Paoletti, A. and Moseley, J. B. (2013). Blt1 and Mid1 provide overlapping membrane anchors to position the division plane in fission yeast. *Mol. Cell. Biol.* **33**, 418-428. doi:10.1128/MCB.01286-12

Head, B. P., Patel, H. H. and Insel, P. A. (2014). Interaction of membrane/lipid rafts with the cytoskeleton: impact on signaling and function. *Biochim. Biophys. Acta* **1838**, 532-545. doi:10.1016/j.bbamem.2013.07.018

Huang, J., Huang, Y., Yu, H., Subramanian, D., Padmanabhan, A., Thadani, R., Tao, Y., Tang, X., Wedlich-Soldner, R. and Balasubramanian, M. K. (2012). Nonmedially assembled F-actin cables incorporate into the actomyosin ring in fission yeast. *J. Cell Biol.* **199**, 831-847. doi:10.1083/jcb.201209044

Iwaki, T., Iefuji, H., Hiraga, Y., Hosomi, A., Morita, T., Giga-Hama, Y. and Takegawa, K. (2008). Multiple functions of ergosterol in the fission yeast Schizosaccharomyces pombe. *Microbiology* **154**, 830-841. doi:10.1099/mic.0.2007/011155-0

Jacquier, N. and Schneiter, R. (2012). Mechanisms of sterol uptake and transport in yeast. *J. Steroid Biochem. Mol. Biol.* **129**, 70-78. doi:10.1016/j.jsbmb.2010.11.014

Jourdain, I., Brzezińska, E. A. and Toda, T. (2013). Fission yeast Nod1 is a component of cortical nodes involved in cell size control and division site placement. *PLoS ONE* **8**, e54142. doi:10.1371/journal.pone.0054142

Kovar, D. R., Kuhn, J. R., Tichy, A. L. and Pollard, T. D. (2003). The fission yeast cytokinesis formin Cdc12p is a barbed end actin filament capping protein gated by profilin. *J. Cell Biol.* **161**, 875-887. doi:10.1083/jcb.200211078

Lacroix, B. and Maddox, A. S. (2012). Cytokinesis, ploidy and aneuploidy. *J. Pathol.* **226**, 338-351. doi:10.1002/path.3013

Laporte, D., Coffman, V. C., Lee, I.-J. and Wu, J.-Q. (2011). Assembly and architecture of precursor nodes during fission yeast cytokinesis. *J. Cell Biol.* **192**, 1005-1021. doi:10.1083/jcb.201008171

Lee, W.-L., Bezanilla, M. and Pollard, T. D. (2000). Fission yeast myosin-I, Myo1p, stimulates actin assembly by Arp2/3 complex and shares functions with WASp. *J. Cell Biol.* **151**, 789-800. doi:10.1083/jcb.151.4.789

Löffler, J., Kelly, S. L., Hebart, H., Schumacher, U., Lass-Florl, C. and Einsele, H. (1997). Molecular analysis of cyp51 from fluconazole-resistant Candida albicans strains. *FEMS Microbiol. Lett.* **151**, 263-268. doi:10.1016/S0378-1097(97)00172-9

Makushok, T., Alves, P., Huisman, S. M., Kijowski, A. R. and Brunner, D. (2016). Sterol-rich membrane domains define fission yeast cell polarity. *Cell* **165**, 1182-1196. doi:10.1016/j.cell.2016.04.037

Mañes, S., Mira, E., Gómez-Moutón, C., Lacalle, R. A., Keller, P., Labrador, J. P. and Martinez, A. C. (1999). Membrane raft microdomains mediate front-rear polarity in migrating cells. *EMBO J.* **18**, 6211-6220. doi:10.1093/emboj/18.22.6211

Marichal, P., Gorrens, J., Laurijssens, L., Vermuyten, K., Van Hove, C., Le Jeune, L., Verhasselt, P., Sanglard, D., Borgers, M., Ramaekers, F. C. S. et al. (1999). Accumulation of 3-ketosteroids induced by itraconazole in azole-resistant clinical Candida albicans isolates. *Antimicrob. Agents Chemother.* **43**, 2663-2670. doi:10.1128/AAC.43.11.2663

Martin, S. G. and Berthelot-Grosjean, M. (2009). Polar gradients of the DYRK-family kinase Pom1 couple cell length with the cell cycle. *Nature* **459**, 852-856. doi:10.1038/nature08054

Matsuo, Y., Fisher, E., Patton-Vogt, J. and Marcus, S. (2007). Functional characterization of the fission yeast phosphatidylserine synthase gene, pps1, reveals novel cellular functions for phosphatidylserine. *Eukaryot. Cell* **6**, 2092-2101. doi:10.1128/EC.00300-07

Maundrell, K. (1993). Thiamine-repressible expression vectors pREP and pRIP for fission yeast. *Gene* **123**, 127-130. doi:10.1016/0378-1119(93)90551-D

Moseley, J. B., Mayeux, A., Paoletti, A. and Nurse, P. (2009). A spatial gradient coordinates cell size and mitotic entry in fission yeast. *Nature* **459**, 857-860. doi:10.1038/nature08074

Ojkic, N., Wu, J.-Q. and Vavylonis, D. (2011). Model of myosin node aggregation into a contractile ring: the effect of local alignment. *J. Phys. Condens Matter* **23**, 374103. doi:10.1088/0953-8984/23/37/374103

Padmanabhan, A., Bakka, K., Sevugan, M., Naqvi, N. I., D'Souza, V., Tang, X., Mishra, M. and Balasubramanian, M. K. (2011). IQGAP-related Rng2p organizes cortical nodes and ensures position of cell division in fission yeast. *Curr. Biol.* **21**, 467-472. doi:10.1016/j.cub.2011.01.059

Padte, N. N., Martin, S. G., Howard, M. and Chang, F. (2006). The cell-end factor pom1p inhibits mid1p in specification of the cell division plane in fission yeast. *Curr. Biol.* **16**, 2480-2487. doi:10.1016/j.cub.2006.11.024

Paoletti, A. and Chang, F. (2000). Analysis of mid1p, a protein required for placement of the cell division site, reveals a link between the nucleus and the cell surface in fission yeast. *Mol. Biol. Cell* **11**, 2757-2773. doi:10.1091/mbc.11.8.2757

Pollard, T. D. and Wu, J.-Q. (2010). Understanding cytokinesis: lessons from fission yeast. *Nat. Rev. Mol. Cell Biol.* **11**, 149-155. doi:10.1038/nrm2834

Rajendran, L. and Simons, K. (2005). Lipid rafts and membrane dynamics. *J. Cell Sci.* **118**, 1099-1102. doi:10.1242/jcs.01681

Ramalingam, N., Zhao, H., Breitsprecher, D., Lappalainen, P., Faix, J. and Schleicher, M. (2010). Phospholipids regulate localization and activity of mDia1 formin. *Eur. J. Cell Biol.* **89**, 723-732. doi:10.1016/j.ejcb.2010.06.001

Riedl, J., Crevenna, A. H., Kessenbrock, K., Yu, J. H., Neukirchen, D., Bista, M., Bradke, F., Jenne, D., Holak, T. A., Werb, Z. et al. (2008). Lifeact: a versatile marker to visualize F-actin. *Nat. Methods* **5**, 605-607. doi:10.1038/nmeth.1220

Rincon, S. A. and Paoletti, A. (2016). Molecular control of fission yeast cytokinesis. *Semin. Cell Dev. Biol.* **53**, 28-38. doi:10.1016/j.semcdb.2016.01.007

Rincon, S. A., Bhatia, P., Bicho, C., Guzman-Vendrell, M., Fraisier, V., Borek, W. E., Alves, F. L., Dingli, F., Loew, D., Rappsilber, J. et al. (2014). Pom1 regulates the assembly of Cdr2-Mid1 cortical nodes for robust spatial control of cytokinesis. *J. Cell Biol.* **206**, 61-77. doi:10.1083/jcb.201311097

Rincon, S. A., Estravis, M., Dingli, F., Loew, D., Tran, P. T. and Paoletti, A. (2017). SIN-Dependent Dissociation of the SAD Kinase Cdr2 from the Cell Cortex Resets the Division Plane. *Curr. Biol.* **27**, 534-542. doi:10.1016/j.cub.2016.12.050

Rippon, W. J. and Fromtling, A. R. (1993). *Cutaneous Antifungal Agents: Selected Compounds in Clinical Practice and Development*. New York: M. Dekker.

Sanglard, D., Ischer, F., Koymans, L. and Bille, J. (1998). Amino acid substitutions in the cytochrome P-450 lanosterol 14alpha-demethylase (CYP51A1) from azole-resistant Candida albicans clinical isolates contribute to resistance to azole antifungal agents. *Antimicrob. Agents Chemother.* **42**, 241-253.

Seveau, S., Eddy, R. J., Maxfield, F. R. and Pierini, L. M. (2001). Cytoskeleton-dependent membrane domain segregation during neutrophil polarization. *Mol. Biol. Cell* **12**, 3550-3562. doi:10.1091/mbc.12.11.3550

Sheehan, D. J., Hitchcock, C. A. and Sibley, C. M. (1999). Current and emerging azole antifungal agents. *Clin. Microbiol. Rev.* **12**, 40-79. doi:10.1128/CMR.12.1.40

Simons, K. and Ikonen, E. (1997). Functional rafts in cell membranes. *Nature* **387**, 569-572. doi:10.1038/42408

Simons, K. and Toomre, D. (2000). Lipid rafts and signal transduction. *Nat. Rev. Mol. Cell Biol.* **1**, 31-39. doi:10.1038/35036052

Sirotkin, V., Beltzner, C. C., Marchand, J.-B. and Pollard, T. D. (2005). Interactions of WASp, myosin-I, and verprolin with Arp2/3 complex during actin patch assembly in fission yeast. *J. Cell Biol.* **170**, 637-648. doi:10.1083/jcb.200502053

Slubowski, C. J., Funk, A. D., Roesner, J. M., Paulissen, S. M. and Huang, L. S. (2015). Plasmids for C-terminal tagging in Saccharomyces cerevisiae that contain improved GFP proteins, Envy and Ivy. *Yeast* **32**, 379-387. doi:10.1002/yea.3065

Snider, C. E., Willet, A. H., Chen, J.-S., Arpağ, G., Zanic, M. and Gould, K. L. (2017). Phosphoinositide-mediated ring anchoring resists perpendicular forces to promote medial cytokinesis. *J. Cell Biol.* **216**, 3041-3050. doi:10.1083/jcb.201705070

Snider, C. E., Willet, A. H., Brown, H. S. T. and Gould, K. L. (2018). Analysis of the contribution of phosphoinositides to medial septation in fission yeast highlights the importance of PI(4,5)P2 for medial contractile ring anchoring. *Mol. Biol. Cell* **29**, 2148-2155. doi:10.1091/mbc.E18-03-0179

Sohrmann, M., Fankhauser, C., Brodbeck, C. and Simanis, V. (1996). The dmf1/mid1 gene is essential for correct positioning of the division septum in fission yeast. *Genes Dev.* **10**, 2707-2719. doi:10.1101/gad.10.21.2707

Solanko, L. M., Sullivan, D. P., Sere, Y. Y., Szomek, M., Lunding, A., Solanko, K. A., Pizovic, A., Stanchev, L. D., Pomorski, T. G., Menon, A. K. et al. (2018). Ergosterol is mainly located in the cytoplasmic leaflet of the yeast plasma membrane. *Traffic* **19**, 198-214. doi:10.1111/tra.12545

Storchova, Z. and Pellman, D. (2004). From polyploidy to aneuploidy, genome instability and cancer. *Nat. Rev. Mol. Cell Biol.* **5**, 45-54. doi:10.1038/nrm1276

Suarez, C., Carroll, R. T., Burke, T. A., Christensen, J. R., Bestul, A. J., Sees, J. A., James, M. L., Sirotkin, V. and Kovar, D. R. (2015). Profilin regulates F-actin network homeostasis by favoring formin over Arp2/3 complex. *Dev. Cell* **32**, 43-53. doi:10.1016/j.devcel.2014.10.027

Takaine, M., Numata, O. and Nakano, K. (2014). Fission yeast IQGAP maintains F-actin-independent localization of myosin-II in the contractile ring. *Genes Cells* **19**, 161-176. doi:10.1111/gtc.12120

Takeda, T. and Chang, F. (2005). Role of fission yeast myosin I in organization of sterol-rich membrane domains. *Curr. Biol.* **15**, 1331-1336. doi:10.1016/j.cub.2005.07.009

Takeda, T., Kawate, T. and Chang, F. (2004). Organization of a sterol-rich membrane domain by cdc15p during cytokinesis in fission yeast. *Nat. Cell Biol.* **6**, 1142-1144. doi:10.1038/ncb1189

Vavylonis, D., Wu, J.-Q., Hao, S., O'Shaughnessy, B. and Pollard, T. D. (2008). Assembly mechanism of the contractile ring for cytokinesis by fission yeast. *Science* **319**, 97-100. doi:10.1126/science.1151086

Wachtler, V., Rajagopalan, S. and Balasubramanian, M. K. (2003). Sterol-rich plasma membrane domains in the fission yeast Schizosaccharomyces pombe. *J. Cell Sci.* **116**, 867-874. doi:10.1242/jcs.00299

Willet, A. H., McDonald, N. A., Bohnert, K. A., Baird, M. A., Allen, J. R., Davidson, M. W. and Gould, K. L. (2015a). The F-BAR Cdc15 promotes contractile ring formation through the direct recruitment of the formin Cdc12. *J. Cell Biol.* **208**, 391-399. doi:10.1083/jcb.201411097

Willet, A. H., McDonald, N. A. and Gould, K. L. (2015b). Regulation of contractile ring formation and septation in Schizosaccharomyces pombe. *Curr. Opin. Microbiol.* **28**, 46-52. doi:10.1016/j.mib.2015.08.001

Wu, J.-Q., Kuhn, J. R., Kovar, D. R. and Pollard, T. D. (2003). Spatial and temporal pathway for assembly and constriction of the contractile ring in fission yeast cytokinesis. *Dev. Cell* **5**, 723-734. doi:10.1016/S1534-5807(03)00324-1

Wu, J.-Q., Sirotkin, V., Kovar, D. R., Lord, M., Beltzner, C. C., Kuhn, J. R. and Pollard, T. D. (2006). Assembly of the cytokinetic contractile ring from a broad band of nodes in fission yeast. *J. Cell Biol.* **174**, 391-402. doi:10.1083/jcb.200602032

Ye, Y., Lee, I.-J., Runge, K. W. and Wu, J.-Q. (2012). Roles of putative Rho-GEF Gef2 in division-site positioning and contractile-ring function in fission yeast cytokinesis. *Mol. Biol. Cell* **23**, 1181-1195. doi:10.1091/mbc.e11-09-0800

Yonetani, A., Lustig, R. J., Moseley, J. B., Takeda, T., Goode, B. L. and Chang, F. (2008). Regulation and targeting of the fission yeast formin cdc12p in cytokinesis. *Mol. Biol. Cell* **19**, 2208-2219. doi:10.1091/mbc.e07-07-0731

Zhang, D., Vjestica, A. and Oliferenko, S. (2010). The cortical ER network limits the permissive zone for actomyosin ring assembly. *Curr. Biol.* **20**, 1029-1034. doi:10.1016/j.cub.2010.04.017

Zhang, D., Vjestica, A. and Oliferenko, S. (2012). Plasma membrane tethering of the cortical ER necessitates its finely reticulated architecture. *Curr. Biol.* **22**, 2048-2052. doi:10.1016/j.cub.2012.08.047

Zhu, Y.-H., Ye, Y., Wu, Z. and Wu, J.-Q. (2013). Cooperation between Rho-GEF Gef2 and its binding partner Nod1 in the regulation of fission yeast cytokinesis. *Mol. Biol. Cell* **24**, 3187-3204. doi:10.1091/mbc.e13-06-0301

Table S1. Table of strains used in this study.

Strain	Genotype	Source or reference
	Figure 1	
AP240	*ade6-M210 ura4-D18 leu1-32 h-*	Laboratory collection
AP5400	*AP240 + pAF12 (pREP3X-Erg25) ade6-M210 ura4-D18 leu1-32*	This study
	Figure 2	
AP5507	*cdr2-EGFP:kanMX6, rlc1-mcherry:natMX6, sid4-mcherry:hphMX6 ade6-M210 ura4-D18 leu1-32*	This study
AP5511	*cdr2-EGFP:kanMX6, rlc1-mcherry:natMX6, sid4-mcherry:hphMX6 + pAF12 (pREP3X-Erg25) ade6-M210 ura4-D18 leu1-32*	This study
AP5718	*blt1-mEGFP:kanMX6, rlc1-mcherry:natMX6, sid4-mcherry:hphMX6 ade6-M210 ura4-D18 leu1-32*	This study
AP5741	*blt1-mEGFP:kanMX6, rlc1-mcherry:natMX6, sid4-mcherry:hphMX6 + pAF12 (pREP3X- Erg25) ade6-M210 ura4-D18 leu1-32*	This study
	Figure 3	
AP5802	*Pact1-lifeact-GFP:leu1+, rlc1-mcherry:Nat, sid4-mcherry:hphMX6 ade6-M210 ura4-D18 leu1-32*	Laboratory collection
AP5806	*Pact1-lifeact-GFP:leu1+, rlc1-mcherry:natMX6, sid4-mcherry:hphMX6 + pAF23 (pREP42X- Erg25) ade6-M210 ura4-D18 leu1-32*	This study
	Figure 4 and Figure S5	
AP5595	*mid1-mEGFP:kanMX6, rlc1-mcherry:natMX6, sid4-mcherry:hphMX6 ade6- ura4-D18 leu1-32*	This study
AP5621	*mid1-mEGFP:kanMX6, rlc1-mcherry:natMX6, sid4-mcherry:hphMX6 + pAF12 (pREP3X- Erg25) ade6- ura4-D18 leu1-32*	This study
AP5629	*2mYFP-rng2:ura4+, rlc1-mcherry:natMX6, sid4-mcherry:hphMX6 ade6- ura4-D18 leu1-32*	This study
AP5665	*2mYFP-rng2:ura4+, rlc1-mcherry:natMX6, sid4-mcherry:hphMX6 + pAF12 (pREP3X- Erg25) ade6-ura4-D18 leu1-32*	This study

AP5598	*GFP-cdc15:kanMX6, rlc1-mcherry:natMX6, sid4-mcherry:hphMX6 ade6- ura4-D18 leu1-32*	This study
AP5640	*GFP-cdc15:kanMX6, rlc1-mcherry:natMX6, sid4-mcherry:hphMX6 + pAF12 (pREP3X- Erg25) ade6-ura4-D18 leu1-32*	This study
	Figure 5	
AP5601	*cdc12-3YFP:kanMX6, rlc1-mcherry:natMX6, sid4-mcherry:hphMX6 ade6-M210 ura4-D18 leu1-32*	This study
AP5635	*cdc12-3YFP:kanMX6, rlc1-mcherry:natMX6, sid4-mcherry:hphMX6 + pAF12 (pREP3X- Erg25) ade6-M210 ura4-D18 leu1-32*	This study
AP6183	*cdc12-3XGFP:kanMX6, rlc1-mcherry:kanMX6, sid4-mcherry:hphMX6 ade6-M210 ura4-D18 leu1-32*	From Bohnert et al., 2013 (KG15568)
AP6193	*cdc12-3XGFP:kanMX6, rlc1-mcherry:kanMX6, sid4-mcherry:hphMX6 + pAF12 (pREP3X-Erg25)ade6-M210 ura4-D18 leu1-32*	This study
AP6129	*cdc12-3YFP:kanMX6, rlc1-mcherry:natMX6, sid4-mcherry:hphMX6 cdc25-22 ade6-M210 ura4-D18 leu1-32*	This study
AP6145	*cdc12-3YFP:kanMX6, rlc1-mcherry:natMX6, sid4-mcherry:hphMX6 cdc25-22 + pAF12 (pREP3X-Erg25) ade6-M210 ura4-D18 leu1-32*	This study
AP6166	*cdc12-3YFP:kanMX6, rlc1-mcherry:natMX6, sid4-mcherry:hphMX6 cdc25-22 mid1::ura4^{+} ade6-M210 ura4-D18 leu1-32*	This study
	Figure 6	
AP5802	*Pact1-lifeact-GFP:leu1+, rlc1-mcherry:natMX6, sid4-mcherry:hphMX6 ade6-M210 ura4-D18 leu1-32*	Laboratory collection
AP5806	*Pact1-lifeact-GFP:leu1+, rlc1-mcherry:natMX6, sid4-mcherry:hphMX6 + pAF23 (pREP42X- Erg25) ade6-M210 ura4-D18 leu1-32*	This study
AP240	*ade6-M210 ura4-D18 leu1-32 h-*	Laboratory collection
AP5400	*AP240 + pAF12 (pREP3X- Erg25) ade6-M210 ura4-D18 leu1-32*	This study
TP1032	*myo1::kanMX6 h- ade6-M210 leu1-32*	from Riken Institute (FY13570)
AP5894	*myo1::kanMX6 + pAF12 (pREP3X-Erg25) ade6-M210 leu1-32*	This study
	Figure S1	

AP240	*ade6-M210 ura4-D18 leu1-32 h-*	Laboratory collection
AP5400	*AP240 + pAF12 (pREP3X-Erg25) ade6-M210 ura4-D18 leu1-32*	This study
AP5323	*erg6Δ::kanMX6 ade6-M210 ura4-D18 leu1-32*	This study
AP5724	*erg6Δ::kanMX6 + pAF12 (pREP3X-Erg25) ade6-M210 ura4-D18 leu1-32*	This study
AP5716	*erg25-ENVY:kanMX6 ade6-M210 ura4-D18 leu1-32*	This study
AP5770	*erg25-ENVY:kanMX6, (SPAC1B2.03c)ER-marker-mcherry:natMX6 ade6-M210 ura4-D18 leu1-32*	This study
AP5790	*erg25-ENVY:kanMX6, rlc1-mcherry:natMX6, sid4-mcherry:hphMX6 + pAF12 (pREP3X-Erg25) ade6-M210 ura4-D18 leu1-32*	This study
AP5808	*scs2Δ::kanMX6 ade6-M210 ura4-D18 leu1-32*	This study
AP5843	*scs2Δ::kanMX6 + pAF12 (pREP3X-Erg25) ade6-M210 ura4-D18 leu1-32*	This study
AP5785	*scs22Δ::kanMX6 ade6-M210 ura4-D18 leu1-32*	This study
AP5793	*scs22Δ::kanMX6 + pAF12 (pREP3X-Erg25) ade6-M210 ura4-D18 leu1-32*	This study
AP5837	*scs22Δ::kanMX6, scs2Δ::natMX6 ade6-M210 ura4-D18 leu1-32*	This study
AP5847	*scs22Δ::kanMx6, scs2Δ::natMX6 + pAF12 (pREP3X-Erg25) ade6-M210 ura4-D18 leu1-32*	This study
	Figure S2	
AP5507	*cdr2-EGFP:kanMX6, rlc1-mcherry:natMX6, sid4-mcherry:hphMX6 ade6-M210 ura4-D18 leu1-32*	This study
AP5511	*cdr2-EGFP:kanMX6, rlc1-mcherry:natMX6, sid4-mcherry:hphMX6 + pAF12 (pREP3X-Erg25) ade6-M210 ura4-D18 leu1-32*	This study
AP3788	*cdr2-tagRFP:natMX6 mid1-mEGFP:kanMX6 ade6-M210 ura4-D18 leu1-32*	Laboratory collection
AP6094	*cdr2-tagRFP:natMX6 mid1-mEGFP:kanMX6+ pAF12 (pREP3X-Erg25) ade6-M210 ura4-D18 leu1-32*	This study
	Figure S3	
AP6184	sid4-GFP:kanMX6, rlc1-mcherry:NatMX6 *ade6-M210 ura4-D18 leu1-32*	This study
AP6155	sid4-GFP:kanMX6, rlc1-mcherry:NatMX6 *+ pAF12 (pREP3X-Erg25) ade6-M210 ura4-D18 leu1-32*	This study
	Figure S4 and S6	

AP5802	*Pact1-lifeact-GFP:leu1+, rlc1-mcherry:natMX6, sid4-mcherry:hphMX6 ade6-M210 ura4-D18 leu1-32*	Laboratory collection
AP5806	*Pact1-lifeact-GFP:leu1+, rlc1-mcherry:natMX6, sid4-mcherry:hphMX6 + pAF23 (pREP42X- Erg25) ade6-M210 ura4-D18 leu1-32*	This study

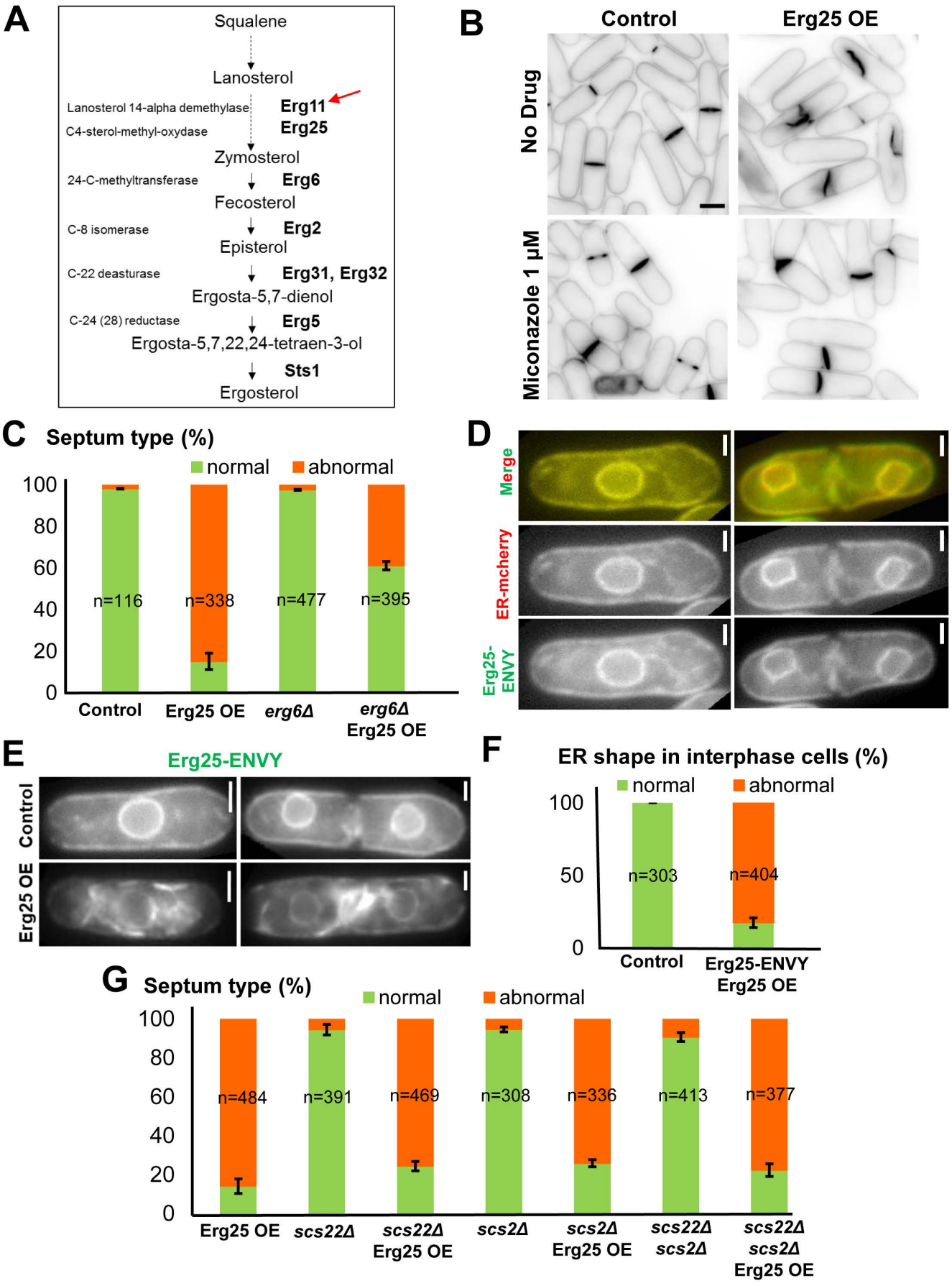

Figure S1. Cytokinetic defects induced by Erg25 OE require an active sterol biosynthetic pathway, while Erg25 affects ER organization with little impact on division plane positioning.

A: Schematic representation of the late stages of ergosterol biosynthetic pathway in *S. pombe* deduced from *S. cerevisiae* (adapted from Iwaki et al., 2008). The red arrow indicates at which level of the pathway miconazole acts. **B:** Calcofluor staining of control and Erg25 OE cells, treated and non-treated with 1µM miconazole. Scale bar, 5µm. **C:** Quantification of septum defects observed by calcofluor staining of control (n=116), Erg25 OE (n=338), *erg6Δ* (n=477) and Erg25 OE *erg6Δ* cells (n=395). Error bars: SD. **D**: Epifluorescence images of Erg25-ENVY and of the ER marker Elo2 fused to mcherry (ER-mcherry). Scale bars: 5µm. **E**: Epifluorescence images of Erg25-ENVY in control (top) and Erg25 OE cells (bottom) in interphase (left) and in late cytokinesis (right). Scale bars: 5µm. **F**: Quantification of ER shape in interphase in control (n=303) and Erg25 OE cells (n=404). Error bars: SD. **G**: Quantification of septum types in Erg25 OE (n=484), *scs22Δ* (n=391), *scs22Δ* Erg25 OE (n=469), *scs2Δ* cells (n=308), *scs2Δ* Erg25 OE (n=336), *scs22Δscs2Δ* (n=413) and *scs22Δscs2Δ* Erg25 OE cells (n=377). Error bars: SD.

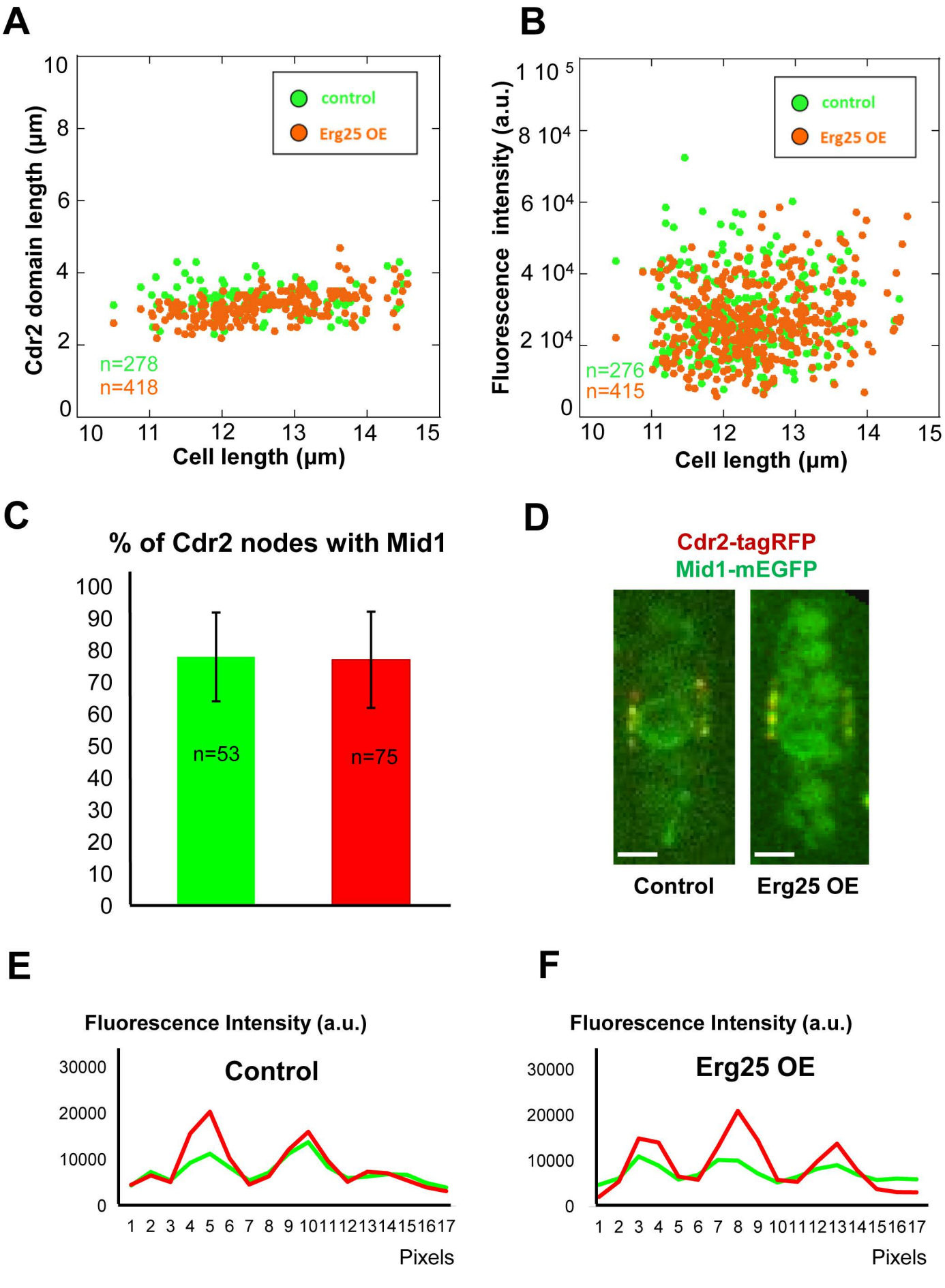

Figure S2. Characterization of Cdr2 and Mid1 domains upon Erg25OE.

A: Length of the Cdr2-EGFP domain relative to cell length in control (n=278) and Erg25 OE cells (n=418). **B:** Integrated fluorescence intensity (a.u.) of Cdr2-EGFP domain relative to cell length in control (n=278) and Erg25 OE cells (n=418). **C:** Percentage of Cdr2-tagRFP nodes containing Mid1-mEGFP in single cells. Error bars: SD (n>50 cells, top right). **D:** Medial planes confocal images of Mid1-mEGFP and Cdr2-tagRFP in control (left) and Erg25 OE cells (right). Scale bar, 5 µm. **E-F**: Linescan analyzing Mid1-mEGFP and Cdr2-tagRFP intensity along the medial cortex (bottom) along the cells shown at the top right.

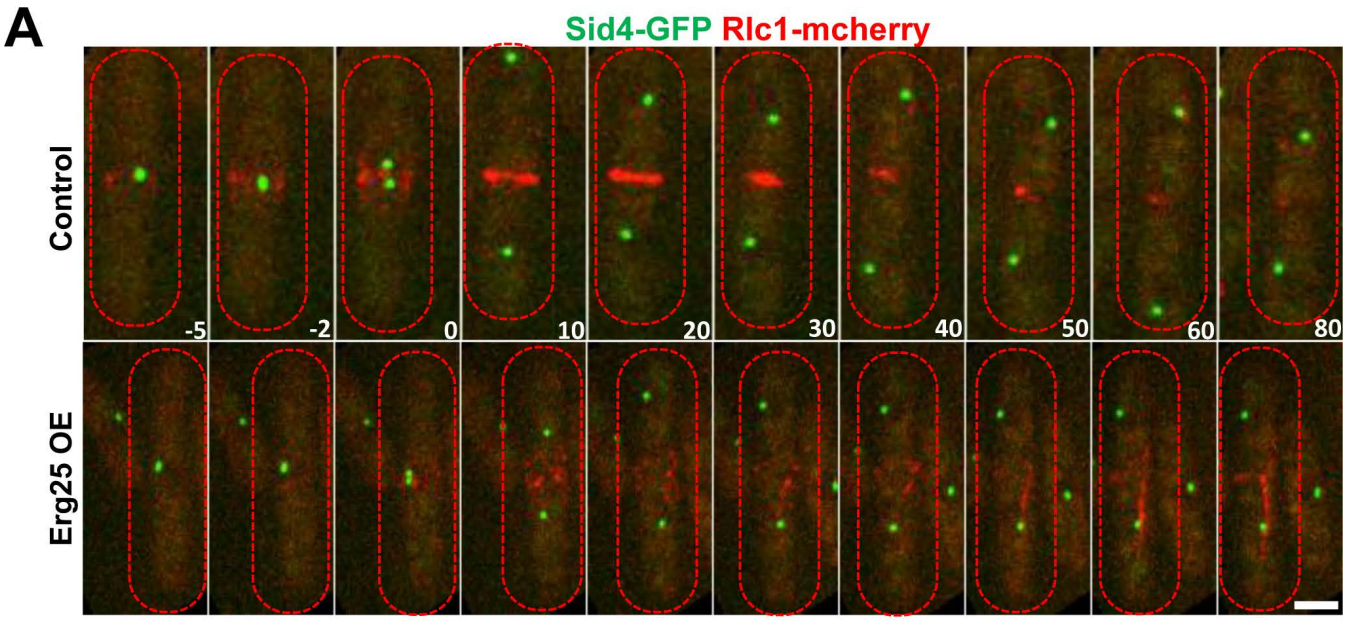

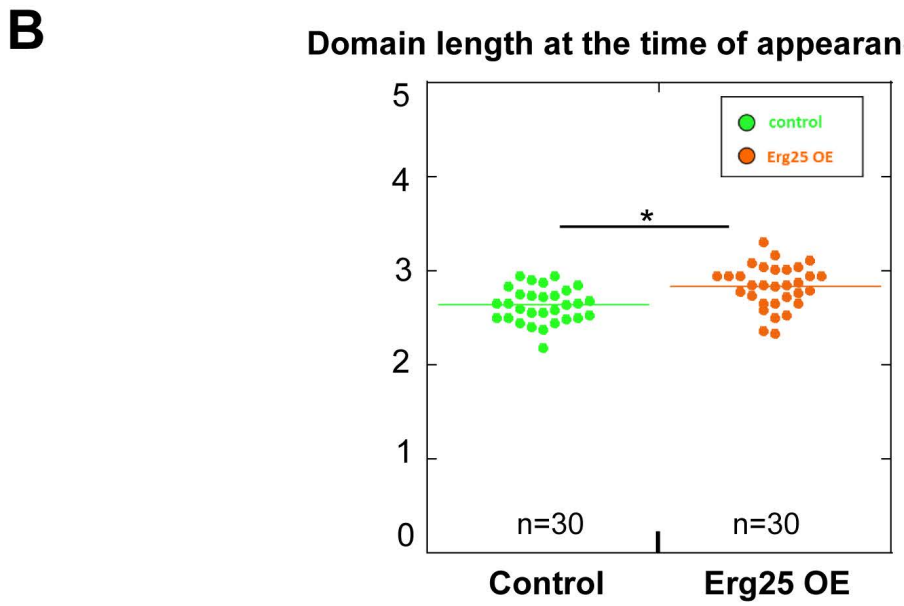

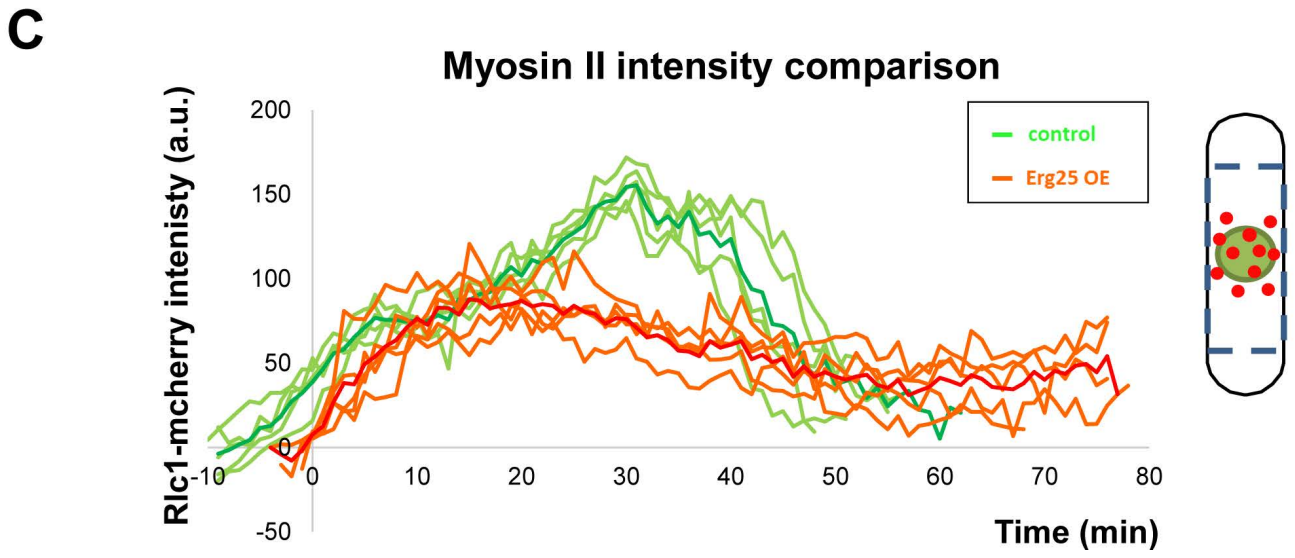

Figure S3. Analysis of myosin II behavior in Erg25 OE cells.

A: Time-lapse analysis of Sid4-GFP and Rlc1-mcherry in control (top) and Erg25 OE cells (bottom). Medial plane confocal images are shown. Time 0 corresponds to mitotic entry. Scale bars: 5 µm. **B:** Measurement of myosin II domain length at the time of its initial recruitment in control and Erg25 OE cells (n=30). **C:** Analysis of myosin II intensity (a.u.) in the central region in control and Erg25 OE cells (n=5). t=0 corresponds to SPB separation.

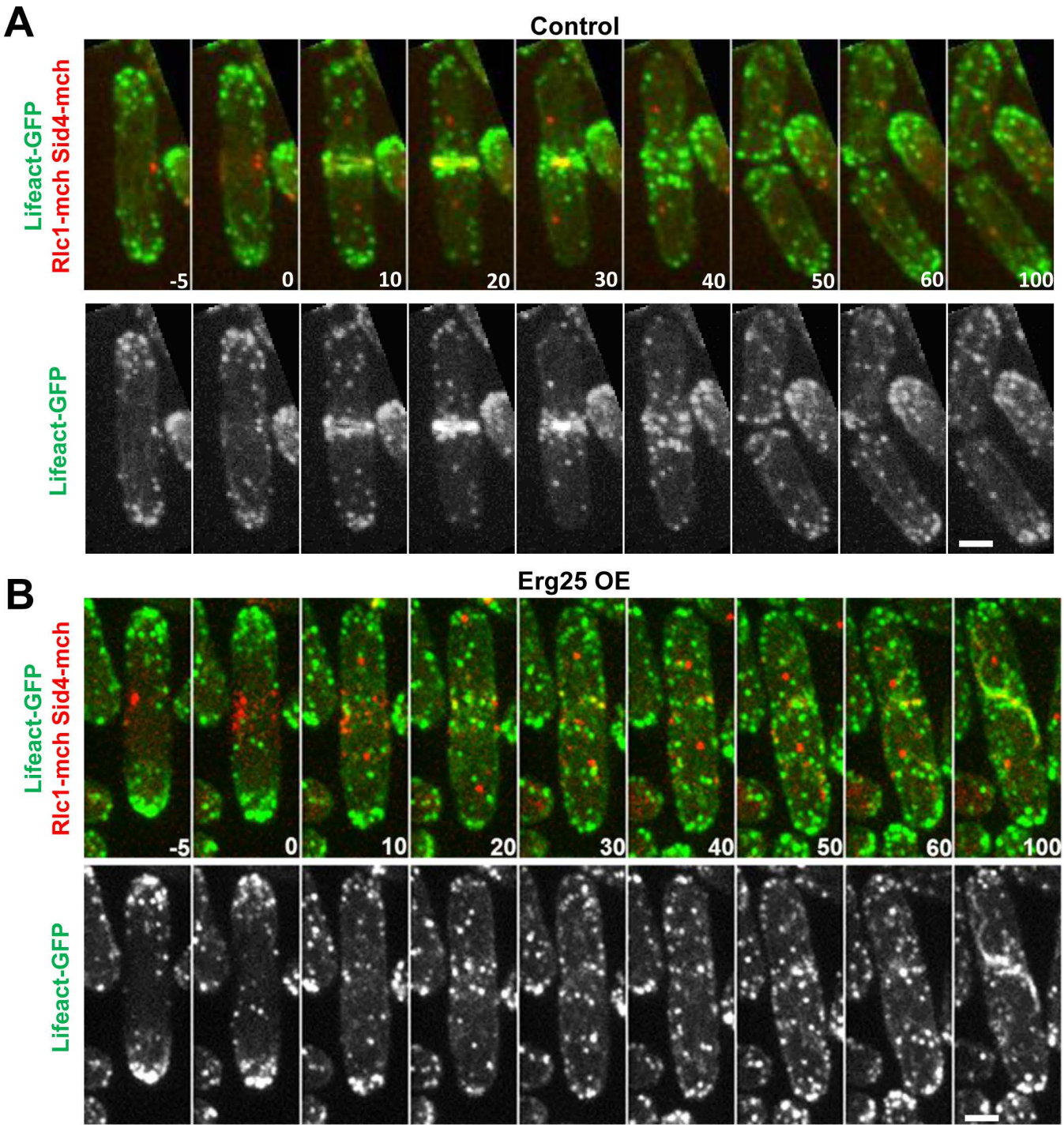

Figure S4: Inhibition of F-actin nucleation from cytokinetic precursor nodes upon Erg25 OE

Time-lapse images of control (**A**) and Erg25 OE cells (**B**) expressing lifeact-GFP, Rlc1-mcherry and Sid4-mcherry. Time 0 corresponds to mitotic entry. Scale bars: 5µm.

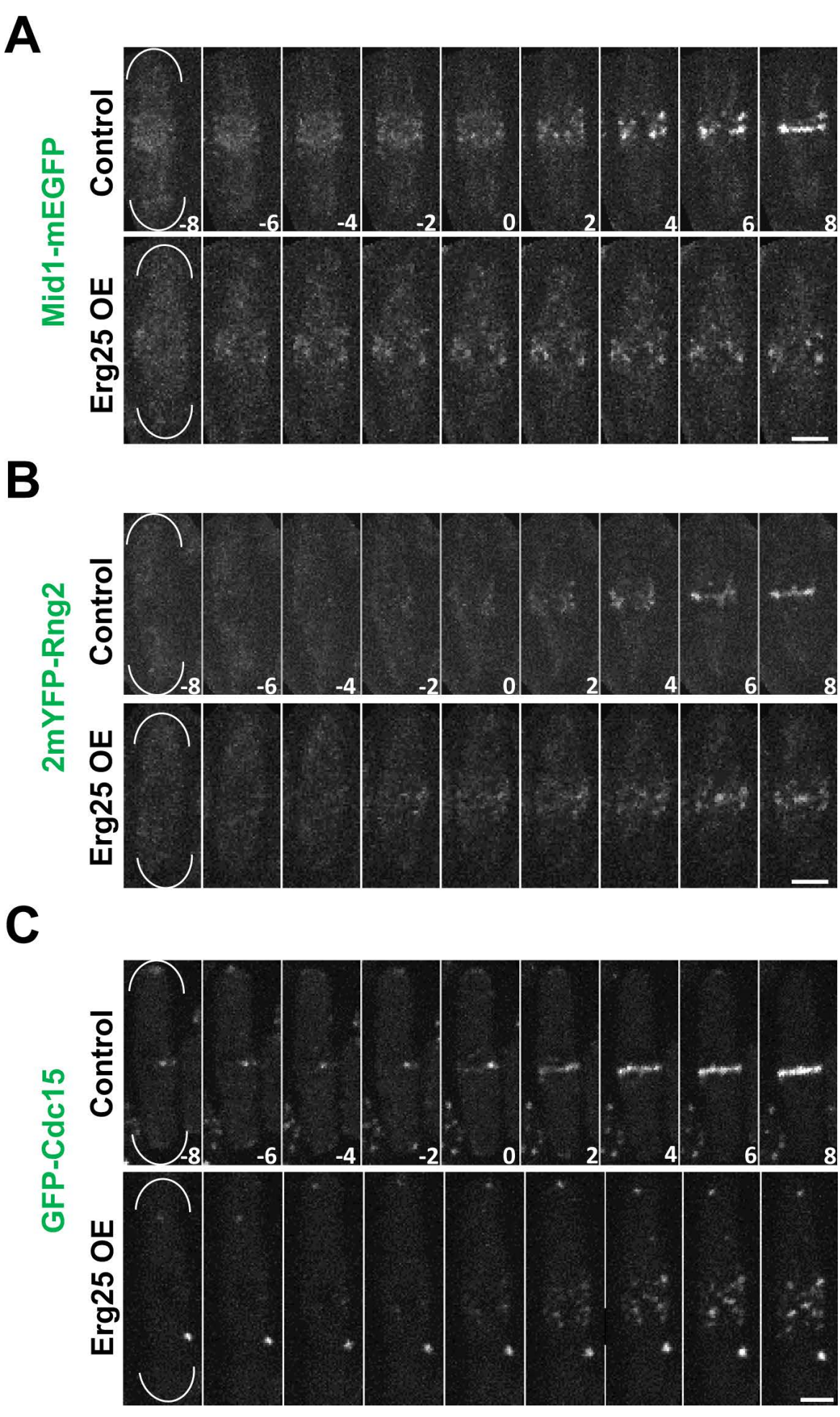

Figure S5. Analysis of Mid1, Rng2 and Cdc15 by time lapse imaging upon Erg25 OE.

Time lapse images of Mid1-mEGFP (**A**), 2mYFP-Rng2 (**B**) and GFP-Cdc15 (**C**) in control (top) and Erg25 OE cells (bottom). Time 0 corresponds to the time of SPB separation. Scale bar, 5 µm.

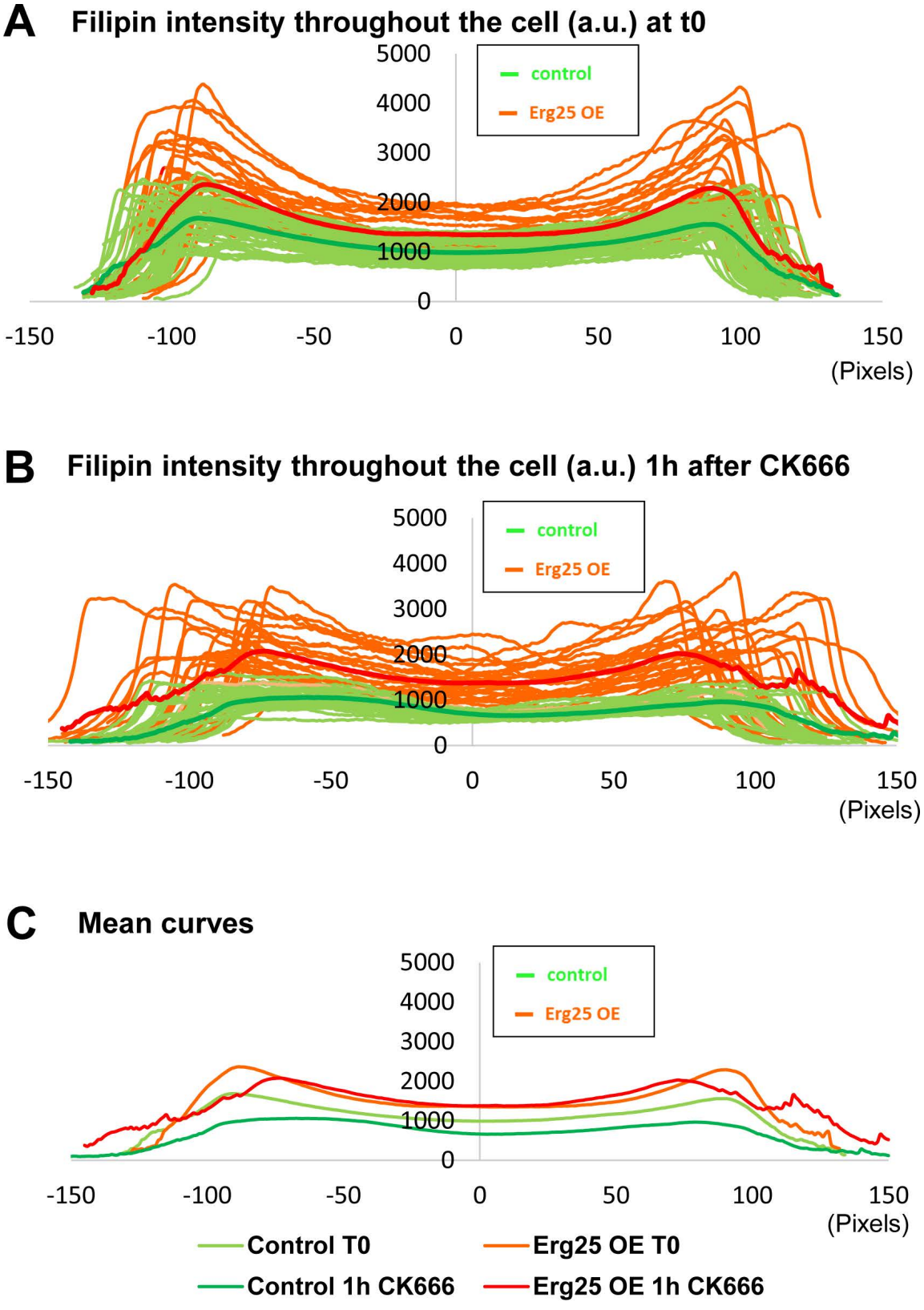

Figure S6. Measurement of Ergosterol levels after treatment with CK666

A-B: Filipin intensity expressed in a.u. was measured in control and Erg25 OE cells at time 0 (**A**) and after 1h of CK666 treatment (n=30 cells) (**B**). **C:** Graph showing the average curves of filipin intensity of control and Erg25 OE cells at time 0 and after 1h treatment with CK666.

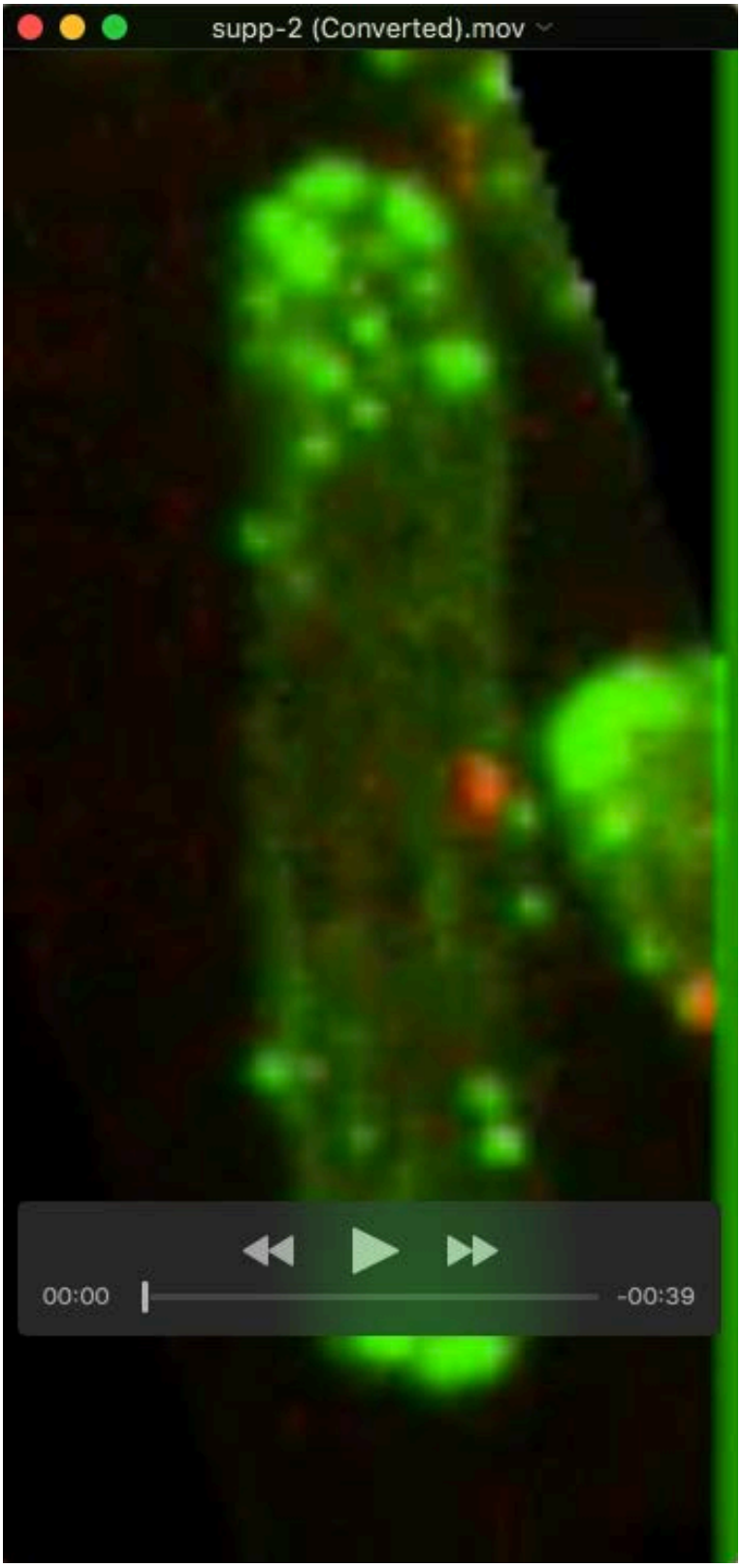

Movie 1. F-actin dynamic distribution in a representative dividing control cell.

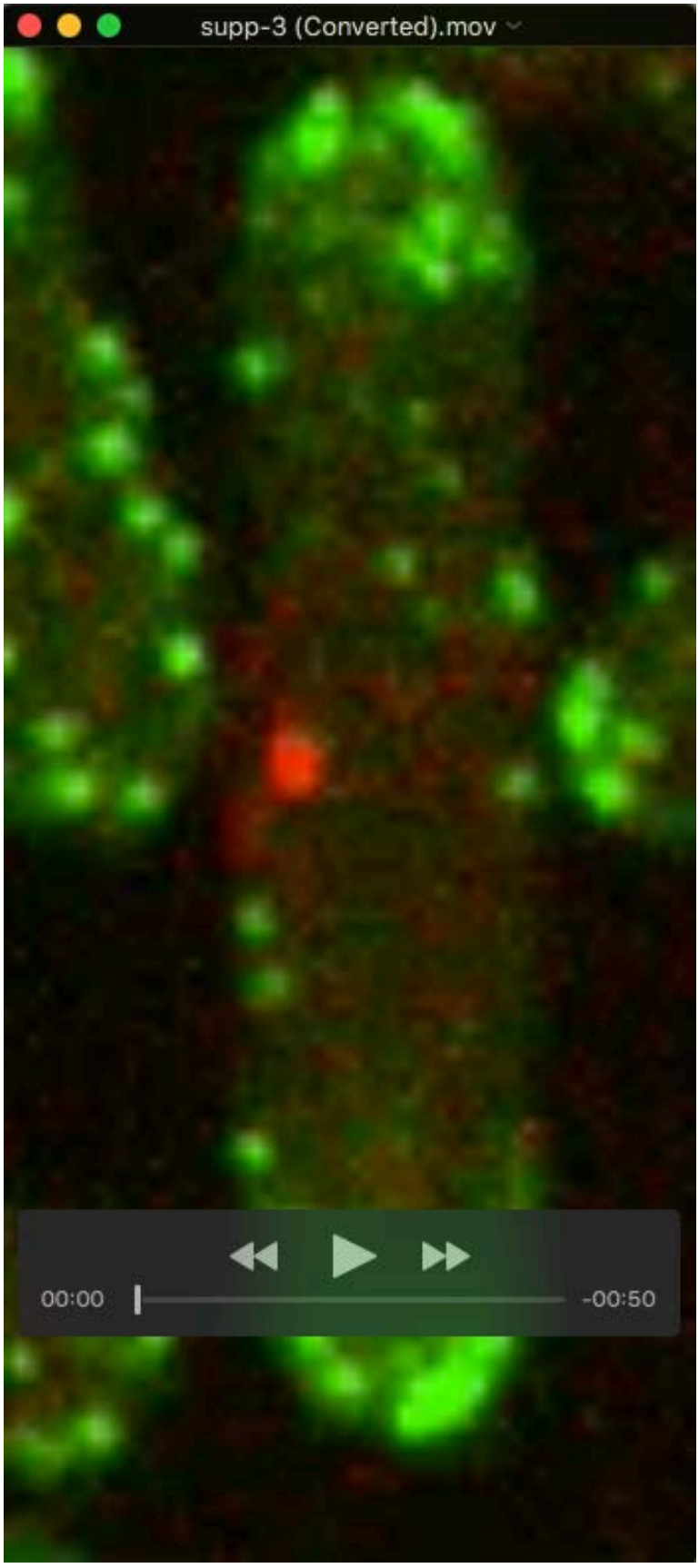

Movie 2. F-actin abnormal organization upon Erg25 OE.

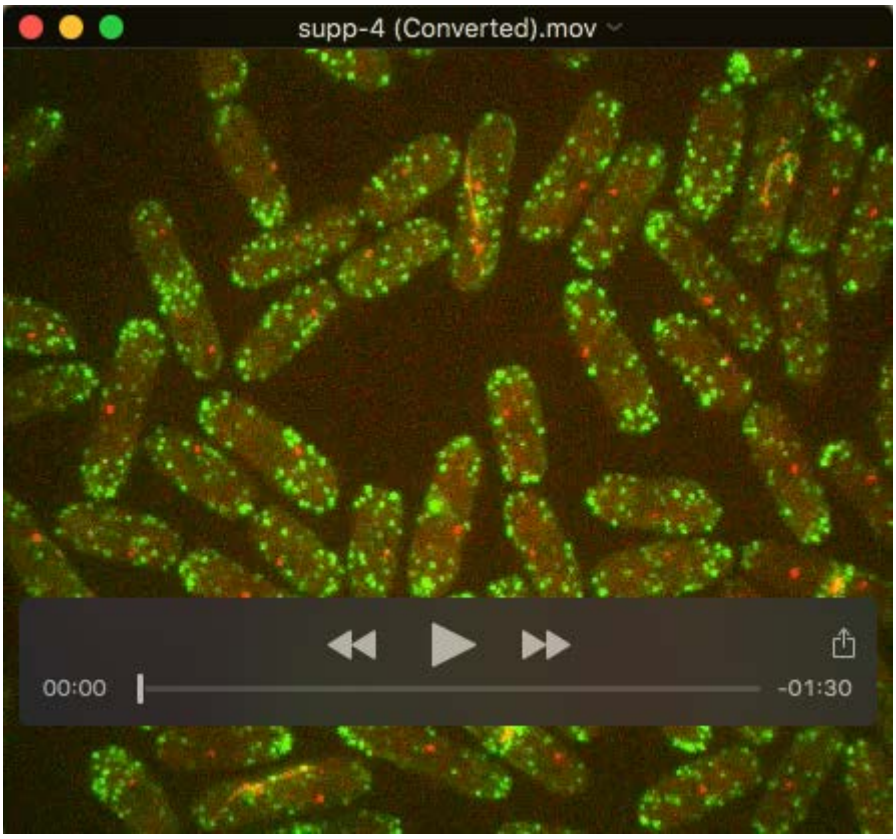

Movie 3. Multiple examples of F-actin aberrant organization upon Erg25 OE in comparison with control cells.